Tyrosyl-DNA phosphodiesterase 1 (TDP1) and SPRTN protease repair histone 3 and topoisomerase 1 DNA-protein crosslinks in vivo

Ivan Anticevic[1], Cecile Otten[1], Luka Vinkovic[1], Luka Jukic[1], Marta Popovic[1]*

[1]Laboratory for molecular ecotoxicology, Institute Ruder Boskovic, Department for Marine and Environmental Research, Zagreb, Croatia

* Correspondence: Marta Popovic
Corresponding Author
mpopovic@irb.hr

Keywords: DNA repair, DNA-protein crosslinks, Tyrosyl-DNA phosphodiesterase 1 (TDP1), SPRTN, zebrafish

Abstract

DNA-protein crosslinks (DPCs) are very frequent and damaging DNA lesions that affect all DNA transactions, which in turn can lead to the formation of DSBs, genomic instability and cell death. At the organismal level, impaired DPC repair (DPCR) is associated with cancer, aging, and neurodegenerative phenotypes. Despite the severe consequences of DPCs, the mechanisms of the DPCR pathway at the organism level are still largely unknown. SPRTN is a protease that removes most cellular DPCs during replication, whereas tyrosyl-DNA phosphodiesterase 1 repairs one of the most abundant enzymatic DPCs, topoisomerase 1-DPC (TOP1-DPC). How these two enzymes repair DPCs at the organism level is currently unknown. Using the zebrafish animal model and human cells, we demonstrate that TDP1 and SPRTN repair endogenous, camptothecin- and formaldehyde-induced DPCs, including histone H3- and TOP1-DPCs. We show that resolution of H3-DNA crosslinks depends on upstream proteolysis by SPRTN and subsequent peptide removal by TDP1 in RPE1 cells and zebrafish embryos, whereas SPRTN and TDP1 function in different pathways in the repair of endogenous TOP1-DPCs.

Introduction

DNA-protein crosslinks (DPCs) are very frequent DNA lesions that are triggered by byproducts of normal cellular processes such as aldehydes, reactive oxygen species, and helical DNA modifications including apurinic/apyrimidinic (AP) sites (Vaz et al., 2017). They occur endogenously at a high frequency, with current estimates of 6000 lesions per cell per day (Ruggiano & Ramadan, 2021b). DPCs can also arise from the exposure to exogenous sources such as UV light, ionizing radiation, and chemotherapeutic agents (Fielden et al., 2018). These bulky lesions vary considerably depending on the type of DNA-binding protein, binding chemistry, and DNA topology near the lesion (single- or double-strand breaks, or intact DNA). Any protein in the vicinity of DNA can be crosslinked upon exposure to the above triggers. Histones, high mobility group proteins, and DNA-processing enzymes such as topoisomerases, DNA (cytosine-5)-methyltransferase 1 (DNMT1), poly [ADP-ribose] polymerase 1 (PARP1), and Ku70/80 have recently been identified as the majority of endogenous cellular DPCs (Kiianitsa & Maizels, 2020). Considering that DPCs affect all DNA transactions including replication, transcription, chromatin remodeling, and DNA repair, the consequences of impaired repair are severe and include single- and double- strand breaks, genomic instability, and apoptosis, which in turn can lead to cancer, accelerated aging and neurodegeneration. In contrast to other DNA repair pathways that have been extensively studied for decades, DPC repair is a relatively new field that was only recognized as a DNA Damage Repair (DDR) pathway in its own right after 2014, when the first protease that initiates DPC removal from the DNA backbone was found in yeast (Wss1) (Stingele et al., 2014a).

DPCs can be repaired by proteolysis followed by removal of the peptide residues from the DNA backbone, or by nucleases excising the part of the DNA to which the crosslinked protein is bound. The majority of cellular DPCs are thought to be removed by the SPRTN protease in dividing cells (Duxin et al., 2014; Maskey et al., 2017; Stingele et al., 2016; Vaz et al., 2016), while the exact contribution of other proteases, including ACRC/GCNA, FAM111A, DDI1, DDI2, and proteasome, remains to be determined (Ruggiano & Ramadan, 2021a). After proteolysis, the remaining crosslinked peptide could be repaired by the nucleotide excision repair pathway (Chesner & Campbell, 2018) or, in the case of crosslinked toposomerases 1 and 2 (TOP1- and 2-DPCs), by tyrosil-DNA phosphodiesterases 1 and 2 (TDP1 and 2) (Pommier et al., 2022).

Topoisomerase 1 and 2 create a transient DNA-protein intermediate to reduce DNA torsional stress. Camptothecin and its derivatives are used in cancer therapy to stabilize TOP1 intermediates and prevent cancer cell replication (Fengzhi Li, 2017). TDP1 is a critical enzyme for TOP1-DPC repair and is a promising target for cancer treatment (Laev et al., 2016, Sun et al., 2020). The phosphotyrosyl bond between TOP1 and DNA is hydrolyzed by TDP1, releasing the TOP1 residue from the DNA backbone (Pommier et al., 2014). This bond is normally shielded and becomes accessible to TDP1 after partial proteolysis of TOP1. However, the dominant protease acting upstream of TDP1 has not yet been identified. While SPRTN has previously been considered the major protease for TOP1-DPC repair (Larsen et al., 2019; Reinking et al., 2020; Vaz et al., 2016), other proteases such as FAM111A, DDI1, and DDI2, as well as the proteasome, have also been associated with TOP1-DPC proteolysis (Kojima et al., 2020; C. P. Lin et al., 2008; Serbyn et al., 2020). Alternatively, another mechanism involving the 3'-flap endonucleases (Mus81/Eme1, Mre11/Rad50, and XPF/ERCC1) can facilitate TOP1-DPC removal without the need for proteolysis (Deng et al., 2005; Liu et al., 2002; Sun et al., 2020; Vance & Wilson, 2001, 2002). However, the nucleolytic pathway may not be as effective in cancer cells which often have mutated or inactivated DNA checkpoints required for endonuclease activation (Dexheimer, 2008), potentially making them more dependent on repair mediated by proteases and TDP1. Point mutations in TDP1 and SPRTN lead to the neurological disorder spinocerebellar ataxia with axonal neuropathy-1 (SCAN1) (Takashima et al., 2002) and Ruijs–Aalfs syndrome (RJALS) characterized by premature aging and early-onset liver cancer (Lessel et al., 2014), respectively.

In addition to tyrosyl residues, purified TDP1 can resolve a variety of substrates at the 3' end of DNA (Interthal et al., 2005; Raymond et al., 2004), and recent data have shown that TDP1 removes histones H2B and H4 from AP sites in the *in vitro* system (Wei et al., 2022) without the need for prior proteolysis. However, TDP1 is unable to remove larger DPCs including Parp1 and TOP1 *in vitro* (Heidrun & James, 2011; Prasad et al., 2019; Wei et al., 2022). It is currently unknown how these discoveries translate to the *in vivo* system. Understanding the role of TDP1 in DPC repair at the cellular and organismal levels could provide an impetus for the development of new drugs and combination therapies with TOP1-DPC inducing drugs. Therefore, we have set out to investigate whether TDP1 can repair histone and TOP1 DPCs in cells and animal model and whether upstream proteolysis by SPRTN is required. Previously, it was thought that TDP1 specifically repairs TOP1-DPC remnants in cells, whereas data at the organism level were lacking. Our model organism is the zebrafish (*Danio rerio*), a well-established vertebrate model used to study cancer, neurodegenerative and cardiovascular diseases (Bradford et al., 2022; Choi et al., 2021). In zebrafish, DNA damage genes and pathways are 99% conserved compared to humans. Unlike mice, zebrafish is externally fertilized, which greatly facilitates gene editing, embryo manipulation, and DPC analysis. In addition, zebrafish are comparatively cheaper to keep and breed, and their very high fecundity allows for better statistical analysis of DPC formation and repair in both, embryos and adults (Choi et al., 2021; C. Y. Lin et al., 2016).

In this study, we investigate the function of TDP1 and SPRTN in the repair of TOP1 and histone H3 DPCs, as well as total cellular DPCs. To this end, we combine knockdown of Sprtn with a Tdp1-deficient zebrafish model and RPE1 cell lines with reduced expression of TDP1 and SPRTN. For this purpose, we developed and verified new tools, including a Tdp1-deficient zebrafish strain, a zebrafish Tdp1 antibody, morpholino probes for *sprtn* silencing in embryos, a modification of the RADAR assay for DPC isolation from zebrafish embryos, and detection of TOP1- and H3-DPCs in embryonic tissues. We

show that TDP1 and SPRTN are required for *in vivo* resolution of TOP1 and H3 DPCs and that both enzymes are also required for repair of other cellular DPCs. In contrast to H3-DPC repair, where SPRTN and TDP1 function together, we show that they work in separate pathways during repair of endogenous TOP1-DPCs. Our results reveal the relationship between TDP1 and SPRTN in the repair of DNA-protein crosslinks (DPCs) in zebrafish, providing the first in-depth insights into the repair of DPCs at the organism level.

Materials and methods

Zebrafish husbandry and chemical treatment of embryos

Zebrafish (*Danio rerio*) AB were purchased from the European Zebrafish Resource Centre (EZRC, Karlsruhe, Germany). Fish were maintained at a constant temperature of 28 ºC and on a 14-hour light and 10-hour dark cycle, with water quality (temperature, pH, and conductivity) monitored daily. Embryos were maintained in E3 media (5 mM NaCl, 0.17 mM KCL, 0.33 mM CaCl2, and 0.33 mM MgSO4) in petri dishes in the incubator at 28 °C until 2dpf. Two-day-old embryos were dechorionated and treated with 10 µM camptothecin (CPT, Alpha Aesar: J62523) for 1 hour or 5 mM formaldehyde (FA, KEMIKA: 0633501) for 30 minutes. All handling and experiments were performed in accordance with the directions given in the EU Guide for the Care and Use of Laboratory Animals, Council Directive (86/609/EEC), and the Croatian Federal Act on the Protection of Animals (NN 135/2006) under the project license HR-POK-023.

Cell culture, siRNA and chemical treatments

HEK293T (Human embryonic kidney cells) and RPE1 (Retinal pigmentosum epithelial cells 1) cell lines were used in this study. Cells were cultured at 37°C in Dulbecco's Modified Eagle's medium (Capricorn, DMEM-HPA) containing 10% FBS (Capricorn, FBS-11A) serum under 5% CO_2. RPE1 cells were seeded at $1x10^4$ cells/mL in 75 cm2 cell culture plates. The siRNAs targeting TDP1, TDP2, and SPRTN (Table 1) were transfected with Dharmafect reagent (Horizon Discovery, T-2005-01) according to the manufacturer's instructions. Cells were incubated for 72 hours; they grew to 80-100% confluence and were collected for the RADAR assay and qPCR experiments. Silencing efficiency was determined by qPCR using the primers listed in Table 4. Before collection, cells were treated with 10 nM CPT for 1 hour in serum-free media or incubated with 1 mM FA for 20 minutes in ice-cold serum-free media.

Table 1. siRNAs used for gene silencing in human RPE1 cells, with concentrations, manufacturers, and catalog numbers.

siRNAs	SEQUENCE	PURPOSE	c(nM) in 10 mL	SOURCE
HsTDP1_siRNA_1	5'CACAAAUGGUCAGCUGAGA3'	Human *tdp1* gene silencing	25	Sigma-Aldrich (PDSIRNA2D)
HsTDP1_smart_pool siRNAs	5'CGAUGAAUCAAAGUGGUUA3' 5'GGACCAGUUUAGAAGGAUA3' 5'CUGGGGUGUUGUAUGUAUU3' 5'GCUAAGGCCUAGAAGGUUA3'	Human *tdp1* gene silencing	10	Horizon Discovery (E-016112-00-0005)

HsTDP2_siRNA_1	5'GCCAAGAGAUUAUUCCUUU3'	Human *tdp2* gene silencing	5	Horizon Discovery (D-017578-02-005)
HsTDP2_siRNA_2	5'GCAAGAGGCUCCAGAGUCA3'	Human *tdp2* gene silencing	5	Horizon Discovery (D-017578-01-005)
HsSPRTN_siRNA_1	5'CAUCAAAGUCAAAAGCGAA3'	Human *sprtn* gene silencing	5	Horizon Discovery (L-015442-02-0005)
HsSPRTN_siRNA_2	5'CAAGGAUAAGUGUAACAGUTT3'	Human *sprtn* gene silencing	5	ThermoFisher (4392420)

Phylogenetic and syntenic analyses and structural modelling

Blast searches were performed using the NCBI database (National Center for Biotechnology Information) and human TDP1 sequence across bacteria, yeast, algae, plants, fungi, invertebrate and chordate species. Full length protein sequences were aligned using the MAFFT (Multiple Alignment using Fast Fourier Transform) alignment algorithm (Katoh et al., 2002). Alignment quality score was assessed using the Guidance2 server and was 0.563, indicating sufficiently high alignment quality for tree building (Penn et al., 2010). The phylogenetic tree was constructed using the Maximum Likelihood method (PhyML software with optimized tree topology, LG model, 8 rates of categories, tree searching operation best of NNI&SPR (Nearest Neighbor Interchange &Subtree Pruning and Regrafting) (Guindon & Gascuel, 2003). Branch support and Alrt values (Approximate likelihood-ratio test) are shown at tree nodes on a scale of 0-1, where 1 is maximum node (Anisimova & Gascuel, 2006). Synteny *Tdp1* gene analysis between zebrafish, human and mouse were performed using Genomicus a browser for conserved synteny synchronized with genomes from the Ensembl database (Louis et al., 2013). Zebrafish Tdp1 was modeled using the Phyre2 workspace (Kelley et al., 2015) and human TDP1 (PDB: c1nopB) as a template. The degree of protein disorder was predicted using the PONDR-FIT software (Xue et al., 2010).

Generation of the *tdp1* mutant zebrafish line

The short guide (sg)RNA (5'GAATGTGGGGGTCTCTTC3') targeting exon 2 (Figure 1A) was selected using the CRISPR scan algorithm (Moreno-Mateos et al., 2015) and was generated as previously described (Modzelewski et al., 2018). A mixture containing 600 ng/uL of Cas9 protein (NEB: M0386) and sgRNA complex at a 1:1 ratio was generated with a total volume of 3 uL, and 1 nL was injected into one cell stage embryos. Three months after injection, when the F0 zebrafish reached adulthood, they were outcrossed to WT, and their progeny was analyzed using High-resolution melting analysis (HRMA) and sequencing to identify founder fish carrying the target mutation with the primers shown in Table S1. Founder fish were crossed and the F1 generation was raised and genotyped. Female and male were found to have a premature stop codon mutation (Figure S 2A), and they were bred to produce the F2 generation harboring two changes in exon 2 of the *tdp1* gene.

sgRNA creation, and microinjecting procedure

To generate a *tdp1* mutant line, we targeted the first exons of zebrafish Tdp1, and the CRISPR scanning algorithm selected (5'GAATGTGGGGGTCTCTTC3') as the sgRNA with the highest score of 54 and a low off-target effect of 4.63 CFD (Moreno-Mateos et al., 2015). The gRNA was generated according to the established protocol of (Modzelewski et al., 2018). Briefly, the sgRNA template was inserted between two short DNA sequences, one containing the T7 promoter and the second sequence complementary to the scaffold template. In the PCR mixture, we combined the guide DNA template for the sgRNA, the IVT_ T7_ F primer that anneals at the beginning of the template (T7 promoter), the scaffold template, and the OLIGO_SCAFF_R primer that sits at the end of the scaffold sequence (Table S1). The PCR product serves as the template for *in vitro* T7 transcription using the MEGAshortscript™ T7 Transcription Kit (Invitrogen™, AM1354). *In vitro* transcription was performed according to the manufacturer's instructions, and the transcribed RNA was purified using the Monarch® RNA Cleanup Kit (NEB, T2040L), RNA concentration was measured, and the guide RNA was stored at -80 °C. On the day of injection, guide RNA was incubated with Cas9 protein in a 1:1 ratio for 5 min at 37 °C. The sgRNA/Cas9 complex was pipetted into a Femtotips needle (Eppendorf, 5242957000) and connected to a microinjector (Eppendorf, FemtoJet® 4x).

Table S1. List of oligonucleotides used for the *tdp1* zebrafish mutant line creation and genotyping. All oligos were purchased from Macrogen (Europe).

OLIGONUCLEOTIDE NAME	SEQUENCE	PURPOSE
IVT_ T7_ F	5’GGATCCTAATACGACTCACTATAG3’	Guide creation
OLIGO_SCAFF_R	5’AAAAAAGCACCGACTCGG3’	Guide creation
SCAFFOLD	5’AAAAAAGCACCGACTCGGTGCCACTTTTTCAAGTTGATAACG GACTAGCCTTATTTTAACTTGCTATTTCTAGCTCTAAAAC 3’	Guide creation
DrTdp1_guide	5’GGATCCTAATACGACTCACTATAGGAATGTGGGGGTCTCTTC GTTTTAGAGCTAGAA3’	Guide creation
DrTdp1_genotype_F	5’GCGTGTGCATGCTGAATCAA3’	Genotyping
DrTdp1_genotype_R	5’AGGAAGCAAACAATTGTACTCTAAA3’	Genotyping

Tdp1 activity assay

The activity assay was performed as described in (Zaksauskaite et al., 2021). Briefly, embryo lysates were incubated with a TDP1 oligonucleotide substrate (5’GATCTAAAAGACT3’) containing a tyrosine at the 3' DNA end and Cy 5 at the 5' end for visualization, which was purchased from Midland Certified Reagent Company. If TDP1 is active, a shift in the size of the oligonucleotide substrate becomes visible, revealing the removal of the tyrosine from the substrate. In brief, two-day-old mutants and WT embryos were deyolked in ice-cold PBS, and pelleted embryos were homogenized twice for 10 seconds (Ultra Turrax T25, IKA - Janke & Kunkel) in 200 µL of lysis buffer (200 mM Hepes, 40 mM NaCl,

2 mM MgCl2, 0.5% Triton X-100 with proteinase inhibitors (leupeptin, aprotinin, chymostatin, pepstatin at a concentration of 1 µg/mL and PMSF at a concentration of 1 mM) and incubated on ice for 30 minutes. The supernatant protein solution (600 ng) was incubated with 2.5 µM labeled oligonucleotide substrate (Midland Certified Reagent Company) in assay activity buffer (25 mM Hepes (pH 8.0), 130 mM KCl, and 1 mM dithiothreitol (DTT)) to a final reaction mixture of 10 uL. The reaction was incubated at 37 ^{o}C for 1 hour, then loading buffer was added, followed by boiling at 90 ^{o}C for 10 minutes. All samples were loaded onto a pre-run 20% homemade urea gel and run at constant voltage (150 V) for approximately 1 hour. The oligonucleotide substrate products were visualized using the ChemiDoc MP Imaging System to detect Cy 5 fluorescence (Bio-Rad, 1708280).

Zebrafish gene silencing with morpholino oligonucleotides

Two morpholino oligonucleotides, one targeting the 5'-UTR region of the zebrafish *sprtn* gene and the other targeting the exon 2-intron 2 boundary were designed to block zebrafish *sprtn* transcription, ordered from Genetools (USA), and used as described in (Nasevicius & Ekker, 2000) (Table 2). 1 nL of the microinjection mixture containing 250 µM of each MO, 0.3M KCl and 0.015% phenol red was injected into each one-cell stage embryo. Two-day-old morphants were collected as follows: i) 5 embryos for QPCR analysis and to check the efficiency of morpholino splice blocking, ii) 30 embryos for RADAR experiments. Total RNA was extracted using the Monarch Total RNA Kit (NEB, T2040) according to the manufacturer's instructions. Equal amounts of RNA were reverse transcribed using the High-Capacity cDNA Kit (Applied Biosystems™, 4368814). The splice-blocking efficiency of morpholino was verified by PCR on 5 ng of cDNA with primer pairs annealing upstream and downstream of the morpholino target (Table 3): the 439 bp amplicon from WT and the 339 bp amplicon from *sprtn* morphants caused by exon 2 skipping were separated by 1% agarose gel electrophoresis. Silencing efficiency was quantified using Image J (Figure S3). The same cDNA was used for QPCR analysis with the primers listed in Table 4.

Table 2. List of morpholinos used to silence *sprtn* expression in zebrafish. The morpholinos were obtained from Genotools (USA).

MORPHOLINO	SEQUENCE	TARGET
DrSprtn_Mo_1	5’ TCGGTCTGCTTTAGTAACAACAGTT3’	5’ UTR
DrSprtn_Mo_2	5’AGAGAGGCATATTTAACCAACCTGA3’	ex2-in2 boundary

Table 3. Primers used to determine the silencing efficiency of the exon skipping morpholino. The primers were obtained from Macrogen (Europe).

PRIMER	SEQUENCE	PURPOSE
DrSprtn_Mo_F	5’ACTGTCCGTCCAGTAAGAGG3’	Determining DrSprtn silencing efficiency

DrSprtn_Mo_R	5'CCACTTGCTTGGTTGATTCTGT3'	Determining DrSprtn silencing efficiency

DPC isolation, detection, and quantification

DPC isolation and detection was performed using the modified RADAR (rapid approach to DNA adduct recovery) assay (Kiianitsa & Maizels, 2013). We modified RADAR assay in order to increase processivity and reduce variability between experiments. We also optimized DPC isolation from zebrafish embryos (1-3 dpf). The main modification included the use of a lyophilizer which substituted TCA precipitation step, thus significantly reducing sample loss and variability between samples. DPC isolation from cells was performed with 8 x10^6 cells grown in a 75 cm^2 cell flask. DPC isolation from 2 dpf embryos was performed as follows: (1) lysis of 30 embryos per condition with pre-warmed lysis buffer (6 M GTC, 10 mM Tris-HCl (pH 6.), 20 mM EDTA, 4% Triton X100, 1% N-lauroylsarcosine sodium, and 1% dithiothreitol) for 10 min at 50 °C; (2) precipitation of DNA with crosslinked proteins by adding an equal volume of 98% ethanol; (3) centrifugation at 10,000 rcf for 10 min at 4 °C; (4) washing the pellet four times with wash buffer (20 mM Tris (pH 7.4), 1mM EDTA, 50 mM NaCl, 50% EtOH) with centrifugation steps at 10,000 rcf at 4 °C; (4) dissolving the pellet in 8 mM NaOH. A 25 µL aliquots of the DPC sample was treated with proteinase K (15 µg, Fisher Scientific, BP1700-100), and the DNA was quantified using Pico Green according to the manufacturer's instructions (Invitrogen, P7581). The DPC samples were normalized to the one with the lowest amount of DNA and treated with DNAse (Millipore, E1014) for 1 h at 37 °C. They were then snap-frozen in liquid nitrogen, submitted to overnight lyophilization, and then dissolved in SDS loading buffer (4 M urea, 62.5 mM Tris-HCl (pH 6.8), 1 mM EDTA, 2% SDS). Total DPCs were resolved by SDS-PAGE gradient gel (5-18%) and detected by silver staining according to the manufacturer's protocol (Sigma Aldrich, PROTSIL1). For specific DPC detection, DPCs isolated from cells were applied to the nitrocellulose membrane (GE Healthcare,10-6000-02) for dot blot analysis, while DPCs isolated from embryos were first resolved by SDS-acrylamide gradient gel (5-18%), transferred to PDF membrane (Roche, 03010040001) and then visualized by Western blotting. To detect the presence of histone H3 or TOP1 in the DPCs, the membranes were immunostained with the specific antibodies. For detection of histone H3, 200 ng of DNA-normalized DPCs were subjected to dot blot or Western blotting, and then immunostained with anti-H3 antibody (Cell Signaling, #9715, 1:3000). For detection of TOP1, DPC equivalent of 500 ng DNA were applied to a dot blot (Bethyl, A302-589A, 1: 1000), and an equivalent of 1 µg of DNA-normalized DPCs was resolved using SDS-acrylamide gradient gel with the addition of 4 M urea (Cell Signaling, #38650, 1 : 1000). DNA detection was performed by applying 2 ng of the sample collected for Pico Green detection to a nylon membrane and detecting with the α-dsDNA antibody (abcam ab27156, 1:7000).

MTT viability test

The MTT colorimetric assay was used as an indicator of cell viability as previously described (Wang et al., 2010). In brief, RPE1 cells were seeded in 24-well plates and transfected with siRNA. After 72 hours, cells were incubated with 100 µl of a 5 mg/mL MTT solution (Alfa Aesar, L11939) for 3 hours. The solution was removed and 500 µL isopropanol (Kemika, 1622601) was added, followed by shaking at 350 rpm for 15 minutes (BioSan, PST -60HL-4, Plate Shaker-Thermostat). Absorbance was measured at 570 nm using a microplate reader (Tecan, Infinite M200).

Quantitative PCR analysis

qPCR analysis was performed with the GoTAQ qPCR mix (PROMEGA, A6001) using primer pairs that span exon-exon boundaries to exclude possible amplification from genomic DNA (Table 4). Target gene expression was normalized to a housekeeping gene, the *ATP 50* gene (Otten et al., 2018), which is expressed equally in all samples (embryonic developmental stages and adult tissues, data not shown). Quantification was performed using the Q-gene (Muller et al., 2002) method and gene expression is expressed as MNE (Mean normalized Expression) where $\boldsymbol{MNE} = \boldsymbol{E(HKG)^{Ct(HKG)}} / \boldsymbol{E(gene)^{Ct(gene)}} \times \mathbf{10^6}$. E (HGK) is the primer efficiency of the housekeeping gene; E (gene) is the primer efficiency of the target gene; Ct (HKG) is the mean Ct value for the housekeeping gene; and C t(gene) is the mean Ct value of the target gene. The expression level of the target gene was then normalized to the housekeeping gene *ATP 50*.

Table 4. List of primers used for human, zebrafish, and mouse QPCR analysis. Primers were purchased from Macrogen (Europe).

OLIGONUCLEOTIDE NAME	SEQUENCE	PURPOSE
HsTDP1_qPCR_F	5'GGGACGCTTGTTTCTTCAGC3'	qPCR expression level for human *TDP1* gene
HsTDP1_qPCR_R	5'TCACCATGCACAAGCAGGAT3'	qPCR expression level for human *TDP1* gene
HsSPRTN_qPCR_F	5'GAGGTGGATGAGTATCGGCG3'	qPCR expression level for human *SPRTN* gene
HsSPRTN_qPCR_R	5'GGGTTCCCTGTTAGTAGCTCG3'	qPCR expression level for human *SPRTN* gene
HsTDP2_qPCR_F	5'CCAGTATACATGGGATACACAAATG3'	qPCR expression level for human *TDP2* gene
HsTDP2_qPCR_R	5'TCTGCTGCTGCTCTGAAAAATA3'	qPCR expression level for human *TDP2* gene
HsATP50_qPCR_F	5'ATTGAAGGTCGCTATGCCACAG3'	qPCR expression level for human *ATP50* gene

HsATP50_qPCR_R	5'AACAGAAGCAGCCACTTTGGG3'	qPCR expression level for human *ATP50* gene
DrTdp1_qPCR_F	5'ACAGATGCTCCTGATTTACCCA3'	qPCR expression level for zebrafish *tdp1* gene
DrTdp1_qPCR_R	5'TGTGCCGTCTGTATGCTGTA3'	qPCR expression level for zebrafish *tdp1* gene
DrSprtn_qPCR_F	5'AATGACAAGTTCTTCTGGGGG3'	qPCR expression level for zebrafish *sprtn* gene
DrSprtn_qPCR_R	5'AAACACCAGCACATAGCGTCA3'	qPCR expression level for zebrafish *sprtn* gene
DrTdp2a_qPCR_F	5'CAGAGTCTCTCCAATGTCAATCCA3'	qPCR expression level for zebrafish *tdp2a* gene
DrTdp2a_qPCR_R	5'TGGGTGCACTTGGTTTCTGT3'	qPCR expression level for zebrafish *tdp2a* gene
DrTdp2b_qPCR_F	5'ATGGATTCAGTCTTCGATGAGG3'	qPCR expression level for zebrafish *tdp2b* gene
DrTdp2b_qPCR_R	5'CTGTCAAGTCAATGCAATCCGC3'	qPCR expression level for zebrafish *tdp2b* gene
DrAtp50_qPCR_F	5'CTTGCAGAGCTGAAAGTGGC3'	qPCR expression level for zebrafish *atp50* gene
DrAtp50_qPCR_R	5'ACCACCAAGGATTGAGGCAT3'	qPCR expression level for zebrafish *atp50* gene

MmTdp1_qPCR_F	5'TTGGAACACACCACACGAAA3'	qPCR expression level for mice *Tdp1* gene
MmTdp1_qPCR_R	5'GGGTTTTCTGGTGCCAGTCT3'	qPCR expression level for mice *Tdp1* gene
MmAtp50_qPCR_F	5'TATGCAACCGCCCTGTACTC3'	qPCR expression level for mice *Atp50* gene
MmAtp50_qPCR_R	5'CCTTCAGGAGTTGCCCTACG3'	qPCR expression level for mice *Atp50* gene

High-resolution melting curve analysis

High-resolution melting curve analysis was used to distinguish mutants from WT fish with differences in dsDNA melting fluorescence. Primer par of Table S1, genomic DNA, MeltDoctor HRM Mastermix (Applied Biosystems™, 4415440) were added to 10 µL PCR mix and fluorescence was detected using StepOnePlus™ Real-Time PCR System (Applied Biosystems™, 4376600). Data were analyzed using High Resolution Melting (HRM) software and melting curve changes were confirmed by sequencing.

Development and verification of a custom-made zebrafish anti-Tdp1 antibody

The peptide N-GALEKNNTQIMVRSYE-C was specifically chosen to detect both zebrafish and human TDP1 proteins and was used to immunize two rabbits followed by affinity purification of serum (Genosphere, UK). To test the specificity of the antibody, we performed western blotting on WT and *tdp1* mutant zebrafish samples, as well as on WT HEK293T cells and HEK293T cells overexpressing human TDP1. Cells were transfected with the recombinant plasmid carrying the human *TDP1* gene (GenScript, OHU22350D) using PEI transfection reagent as previously described (Popovic et al., 2013; Tom et al., 2008). Cells were collected after 72 hours and lyzed in RIPA buffer (150 mM NaCl, 1% Triton X-100, 0.50% Na-deoxycholate, 0.10% SDS, 50 mM TrisHCl (pH 8) followed by a 10-second sonication. 2dpf zebrafish embryos were lyzed in RIPA buffer and sonicated twice for 10 seconds. 30 µg of protein extract from cells and 50 µg from zebrafish embryos were loaded on an SDS acrylamide gel, transferred to a PVDF membrane, blocked with milk for 2 hours, and incubated overnight with the custom-made anti-TDP1 antibody (1:1000). The blot was visualized by incubating the membrane with an HRP-labelled anti-rabbit antibody followed by detection using ECL (Biorad) at the Chemidoc (Biorad).

Western blotting and Dot blotting

The cell/embryo lysates and isolated DPCs were mixed with 5x Laemmli buffer containing 50 mM Tris-HCl (pH 6.8), 2% SDS, 10% w/v glycerol, 0.05% bromophenol blue, and 5% β-mercaptoethanol. Additionally, the cell or embryo lysates were boiled for 10 minutes at 90° C. The proteins were then separated by 5-18% SDS-PAGE gradient gels and transferred to PVDF membranes. Specific DPCs in cells were detected using a dot blot (Bio-Rad, Bio-Dot Apparatus 1706545) and transferred directly to a nitrocellulose membrane by vacuum aspiration. The membranes were blocked with 5% low-fat milk

(Roth, T145.1) in TBST buffer (10 mM Tris-HCl (pH 7.5), 15 mM NaCl, 0.02% Tween 20) for 2 hours at room temperature and then incubated with the corresponding primary antibody in 2.5% BSA in TBST overnight at 4°C. The membranes were then incubated with an HRP-labeled anti-rabbit antibody (Sigma-Aldrich. a0545, 1:100000) for 1 hour and washed three times for 15 minutes in TBST. Detection was performed according to the manufacturer's instructions for the ECL blotting substrate (Bio-Rad, 1705061) and visualized using the ChemiDoc™ XRS+ System (Bio-Rad, 1708299).

Statistical Analysis

The ImageJ software (Abràmoff et al., 2004) was used to quantify dot blots, western blots, and morpholino-mediated silencing efficiency in zebrafish. Graphical representation of the expression data and statistical analysis was conducted using the unpaired two-sided Student's t-test using GraphPad Prism 8. Differences between two independent variables were considered significant when $p < 0.05$. All experiments were performed three to five times following the setup for biological replicates for RADAR isolation from cells and embryos, with means ± SD shown in each column.

Results

Comparison of zebrafish, mouse and human TDP1 proteins: phylogeny, synteny, sequence and structure

We constructed a phylogenetic tree of Tdp1 orthologs in multicellular organisms, yeast, and bacteria by aligning protein sequences using the MAFFT algorithm (Katoh et al., 2002) and building a phylogenetic tree using Maximum Likelihood method (Guindon & Gascuel, 2003). The Tdp1 protein is remarkably conserved in all 'kingdoms' of life, from bacteria and yeast to plants and animals and is always present as a single ortholog (Figure 1 and Table S2). Interestingly, the Tdp1 orthologs in invertebrates form two distinct clusters, one which is phylogenetically very close to the vertebrate Tdp1 cluster and the other which is closer to the yeast and bacterial Tdp1 orthologs (Figure 1B). Human and zebrafish Tdp1 are phylogenetically very close (Figure 1B) and structurally very similar (Figure 1A). We modeled the structure of zebrafish Tdp1 using the crystal structure of human TDP1 (PDB: c1nopB) (Davies et al., 2002) in the Phyre2 workspace (Kelley et al., 2015). These orthologs share a very similar structure of N and C domains with a remarkable degree of conservation (Figure 1A). N domain (164. – 358. amino acid) and C domain (359. – 616. amino acid) form a pseudo-2-fold axis of symmetry with each domain contributing histidine, lysine and asparagine to the active site: H263, K265, and N283 in the N domain and H493, K495, and N516 in the C domain (Davies 2022, Flett 2018) (Figure 1A). Upstream of the N domain, is an N terminal portion which is heavily disordered in both zebrafish and human TDP1 (1-163. and 1-144. amino acids, respectively) (Figure S1B). This part is highly variable among species, and its structure has not yet been solved. The amino acid sequence similarity between human and zebrafish Tdp1 is 66% (identity 55%), whereas the similarity between mouse and human is 83% (identity 77%). If we exclude the variable N terminus, similarities between orthologs are much higher: 76% between human and zebrafish (identity 66%) and 92% between human and mouse (identity 88%). After determining the phylogenetic, structural, and sequence similarities between the human, mouse, and zebrafish Tdp1 proteins, we analysed the gene environment of the orthologs. The zebrafish *tdp1* gene is located on chromosome 17, and the upstream neighboring gene *kcnk13a* and the downstream neighboring genes *efcab1*1 and *foxn3* show a syntenic relationship with the human and mouse *TDP1* gene, which are located on chromosome 14 and 12, respectively (Figure 1 C). Apart from the aforementioned neighboring genes, the gene environment between zebrafish on one side and human and mouse *TDP1* on the other side is not conserved. In contrast, the gene environment of *TDP1* in humans and mice exhibits preserved genomic order that was presumably passed down from a common ancestor (Figure 1 C).

Generation and characterization of zebrafish line lacking Tdp1 protein

We used CRISPR/Cas9 system to generated a zebrafish line lacking the Tdp1 protein. A gRNA targeting exon 2 induced a frameshift mutation that resulted in a premature stop codon at amino acid position 44 upstream of catalytic residues H270, K272, and N290 in the N domain (Figures 1A and 2A). The gRNA/Cas9 complex was injected into one-cell stage embryos and fish were grown to adulthood. Identified founder fish in the F0 generation that produced germlines with a frameshift mutation that resulted in premature stop at amino acid position 44 were crossed and the F1 generation was raised. When the F1 generation reached adulthood, individuals were genotyped based on fin tissue and allele changes were sequenced. Females and males carrying described frameshift mutations (Figures 2A and S2A) were further crossed to produce an F2 generation deficient in Tdp1 protein (Figure 2A). The lack of functional Tdp1 protein was confirmed by enzyme activity assay (Figure 2B) and Western blot using a custom-designed antibody for zebrafish Tdp1 (Figures 2C and S2B). For the activity assay, we used a model substrate of Tdp1, a 3'-phosphotyrosyl-DNA probe with a fluorescent reporter Cy-5 at the 5' end (3'pY). When Tdp1 is active, tyrosine is removed from the substrate, resulting in the oligonucleotide form (3'P) (Figure 2B). Lysates from WT embryos (with active TDP1) were incubated with the labeled substrate and very efficient tyrosine removal was observed, whereas no reaction occurred after incubation with the lysates from *tdp1* mutant embryos demonstrating the absence of Tdp1 in the mutants (Figure 2B). Using the custom-made Tdp1 antibody, we showed that the Tdp1 protein is indeed absent in the *tdp1* mutant line (Figure 2C). The zebrafish antibody was intentionally designed with an epitope in a conserved protein region that overlaps between zebrafish and human TDP1 so that it could also be used to detect TDP1 in human cells. Thus, we were able to test the specificity of the new antibody by overexpressing human TDP1 in HEK293 cells (Figure S2B). After determining that the Tdp1 protein was indeed absent in the *tdp1* mutant line (Figure 2C), we examined whether Tdp1 deficiency resulted in phenotype changes in embryos and adult zebrafish. There were no obvious morphological differences between WT and *tdp1* mutant embryos, nor in adult zebrafish that are now 8 months old (Figures 2D and E). Future studies are needed to investigate specific phenotypes in adult Tdp1-deficient zebrafish, particularly with regard to neurodegeneration in old fish.

Tdp1 is highly expressed throughout the embryonic development and in adult tissues

WT embryos were collected at different time points, starting at 6 hours post fertilization (hpf), when most of the maternal transcriptome is degraded (Mathavan et al., 2005). We show that Tdp1 is strongly expressed throughout embryonic development from 6 hpf to 5 days postfertilization (dpf) (Figure 3A). Expression levels are highest at early stages, at 6 hpf and 1 dpf, followed by a 5-fold decrease at later stages (2-5 dpf). Overall, the expression level remain high from 6 hpf to 5 dpf (Figure 3A). To facilitate comparison of expression levels, we set arbitrary thresholds following previous publication (Loncar et al., 2016): high expression when MNE is > 60 x 10^6 (Ct values > 22), moderate when MNE is 2 x 10^6 – 60 x 10^6 (Ct = 23 - 26), and low when MNE is < 2 x 10^6 (Ct > 27). Sprtn shows a similar pattern to Tdp1 at later stages, with high and stable expression levels at 2 to 5 dpf (Figure 3A). Sprtn expression is particularly high at the 6-hpf stage, when levels are 33-fold higher than those of Tdp1.

In adults, Tdp1 is highly expressed in all tissues analysed, with the highest expression in testis and ovary, followed by a 3.3-fold lower expression in brain and kidney and a 14.7-fold lower expression in liver and intestine (Figure 3B). Sex differences are not significant except in the gonads, where Tdp1 is expressed 1.3-fold more in the ovaries than in the testes.

To compare Tdp1 expression in zebrafish with the most commonly used animal model, the laboratory mouse, Tdp1 expression was measured in the corresponding mouse tissues (Figure 3C). The expression pattern is generally similar to that of the zebrafish with the highest expression in the gonads, followed by the brain, liver, kidney, and female intestine. However, there are some differences between the two animal models: (1) overall expression levels is much lower in mice, with

moderate expression in testis and low expression in all other tissues, in contrast to the high expression in all zebrafish tissues; (2) in mice, Tdp1 is expressed 17.2-fold less in ovaries than in testes, in contrast to 1.3-fold higher expression in zebrafish ovaries compared with testes; and finally, (3) a sex difference in Tdp1 expression in mouse intestine was not observed in zebrafish (Figure 3C).

Loss of Tdp1 causes accumulation of DPCs in zebrafish embryos

Tdp1 mutants have significantly higher endogenous DPC levels than WT embryos. The change is 1.4-fold increase and is statistically significant (Figures 4A and 4B, n = 4). All experiments in embryos were repeated 4-6 times (biological replicates), because the results showed higher variability compared to experiments in RPE1 cells. CPT treatment had no effect on total DPC levels in WT embryos, but caused a very large increase (1.7-fold) in *tdp1* mutants (Figures 4A and B). In contrast, the general DPC inducer, FA caused a similar increase in total DPCs independent of Tdp1 deficiency: 2.2-fold in WTs and 2.1-fold in *tdp1* mutants (Figures 4A and 4B).
Following the analysis of the endogenous and exogenous total DPC levels in *tdp1* mutants, we investigated the interplay of Tdp1 and Sprtn in DPC removal at the *in vivo* level. Knockdown of *sprtn* using the morpholino approach reduced *sprtn* mRNA levels by 80% (Figure S3A and B) and resulted in a strong and significant increase in total DPC levels in both, WT and *tdp1* mutant embryos (2.4-fold and 2.5-fold, respectively). Compared with untreated WT embryos, CPT exposure increased total DPCs in *sprtn*-silenced embryos, by 2.6-fold in WT and by 3.1-fold in *tdp1* mutants (Figure 4B). Compared with total DPC levels measured in WT CPT-treated and *tdp1* mutant CPT-treated embryos, we observed significant increases ($p < 0.001$) caused by *sprtn* knockdown in both cases (Figure 4B). However, the effect of *sprtn* silencing on DPC levels was not significant in either WT ($p > 0.05$) or mutant embryos ($p > 0.05$) when exposed to the general DPC inducer, FA (Figure 4B).
Analysis of total cellular DPCs revealed important details about the functions of TDP1 and SPRTN in DPC removal and the effects of DPC inducers. However, to determine which group of DPCs is more affected by these changes, DPCs were divided into three groups: High Molecular Weight (HMW > 151 kDa), Medium Molecular Weight (MMW, 40 kDa to 150 kDa), and Low Molecular Weight (5 - 40 kDa). We are aware that these categorization is not ideal, but it can provide valuable additional information for the analysis of cellular DPCs compared to the analysis of total DPC levels. More detailed analysis revealed that the 1.4-fold increase in total endogenous cellular DPCs in the *tdp1* mutants was indeed due to the increase in low and medium molecular weight DPCs, whereas high molecular weight DPCs were unaffected (Figure 4A, high exposure). Specifically, Tdp1-deficient embryos accumulated 1.7-fold more endogenous LMW DPCs and 1.6-fold more endogenous MMW DPCs than WT embryos (Figures 4C and D). CPT treatment further increased LMW DPC levels: 3.1-fold in mutants and 1.5-fold in WTs (Figure 4C). A different pattern was observed after induction of general DPCs by FA, where levels of LMW DPCs increased 2.5- to 2.7-fold in both WT and mutant embryos (Figures 4A and C). As expected, treatment with FA had strong effects on LMW DPC levels considering that most of cellular DPCs are histones (Kiianitsa & Maizels, 2020). Unexpectedly, LMW DPCs were also induced by CPT treatment (1.5-fold), although not as strongly as after FA treatment. When *sprtn* was knocked down, WT embryos accumulated more LMW DPC (3.1-fold) than mutants (2.4-fold) (Figures 4A and C). CPT treatment further increased LMW in mutant embryos 3.1- fold, but had no effect on LMW levels in WT embryos after knockdown of *sprtn*. LMW levels were not further affected by FA treatment when *sprtn* was silenced in WT or tdp1-deficient embryos (Figure 4 C).
CPT treatment of *tdp1* mutants strongly increased the levels of MMW DPCs (by 2.9-fold), in contrast to a slight statistically nonsignificant change in WT embryos (Figure 4 D). FA increased MMW DPCs by 2.6-fold in mutants and by 4.1-fold in WT embryos, showing a similar pattern of induction as LMW but with much stronger absolute changes. MMW DPCs increased 4.1-fold in both WT and *tdp1* mutants after *sprtn* knockdown (Figure 4D). MMW DPCs in WT embryos and *tdp1* mutants were not additionally affected by CPT or FA treatment in *sprtn* knockdowns (Figure 4 D).
Tdp1 deficiency, *sprtn* knockdown, and exposure to CPT or FA had the least effect on HMW DPCs. However, some of the effects were still pronounced. HMW DPCs increased following *sprtn* knockdown

by 1.5-fold in *tdp1* mutant embryos ($p < 0.05$) and by 2-fold in WT embryos ($p > 0.05$) (Figure 4E). HMW DPCs increased 1.9-fold in the *tdp1* mutant and 1.6-fold in WT when *sprtn* knockdown was combined with CPT treatment. Independent of Tdp1 deficiency, knockdown of *sprtn* showed a similar induction by 1.8-fold in both the *tdp1* mutant and WT embryos which were treated with FA (Figure 4E). Minor variations in HMW DPCs observed between the *tdp1* mutant and WT embryos with and without CPT or FA treatment were not statistically significant.

Loss of Tdp1 causes DPC accumulation in cells

We silenced TDP1 and SPRTN in human RPE1 cells and quantified cellular DPC levels. Silencing of TDP1 alone caused a small, but statistically significant increase in total DPC levels (1.2-fold) (Figure 5A and B), whereas silencing of SPRTN caused a larger, 1.6-fold increase in DPC levels (Figure 5 A and B) (n = 4). The silencing efficiencies of TDP1 and SPRTN were 62% and 65%, respectively (Figure S 4A). When both, TDP1 and SPRTN were silenced (Figure S4 A), we observed an additive effect: a 2-fold increase in total cellular DPCs (Figure 5A and B). Considering that SPRTN is involved in the removal of very diverse DPCs, ranging from low molecular weight (LMW) proteins such as histones to bulky high molecular weight (HMW) proteins such as topoisomerases (Vaz et al., 2016), we further investigated the size distribution of the isolated DPCs. TDP1 silencing increased low and medium molecular weight (LMW and MMW) DPCs by 1.3- and 1.5-fold, respectively (Figures 5A right panel, 5C and S4B). The effect of the increase is not as strong as that of SPRTN silencing, which showed an increase of 2.6-fold in the LMW region and 1.9-fold in the MMW region (Figure 5C). The silencing combination showed an additive effect on the increase in LMW and MMW DPCs (3.2- and 2.2-fold, respectively). The silencing combination also showed a 1.7-fold increase in HMW DPCs, in contrast to single gene silencing, where no increase was observed (Figures 5A and 5C).
After analyzing DPC accumulation in untreated cells, we quantified DPCs after exposure to camptothecin (CPT), a specific TOP1 DPC inducer, and after exposure to formaldehyde (FA), a strong general DPC inducer. We used 10 nM CPT (1 h, 37 °C) in serum-free medium which induces TOP1-DPCs without the occurrence of double-strand breaks (Ray Chaudhuri et al., 2012) and 1 mM FA in serum-free medium (20 min, 37 °C) which induces DPCs and probably also single- and double-strand breaks based on the data from HEK293 cells (Mórocz et al., 2017). Treatment with CPT had a similar effect on DPC accumulation as TDP1 silencing: the total number of DPCs was increased by 1.3-fold, with the largest effect on LMW DPC with a 1.6-fold increase (Figures 5D and 5E). When CPT was added to TDP1-silenced cells, a 1.4-fold increase in total DPCs was observed (Figure 5E), again with the largest effect on LMW with a 1.6-fold increase (Figures 5D and 5F). CPT exposure of SPRTN-silenced cells caused very strong DPC accumulation (2.7-fold compared with untreated WT cells), again with the largest effect on LMW DPCs of 2.-fold increase (Figures 5D, 5E and 5F). In contrast to untreated cells, treatment with CPT after double silencing had no additional effect on DPC accumulation (Figures 5D and 5E). Similar to LMW DPCs, treatment with CPT resulted in a slight 1.3-fold increase in MMW DPCs by. Interestingly, MMW DPCs in cells with silenced TPD1, SPRTN, or TDP1 and SPRTN were equally affected whether CPT was applied or not (Figure S4C). The CPT exposure had the least effect on HMW DPCs (Figure S4C).
In contrast to the DPC response to CPT treatment, the pattern of DPC accumulation after FA treatment was very different. FA treatment increased total DPC levels by 2-fold in all samples regardless of which gene was silenced (Figures 5G and 5H). In all samples, FA treatment had the greatest impact on LMW and MMW DPCs, which increased by 2.3 and 2.8-folds on average in comparison to untreated WT cells (Figure 5I). Proteins of high molecular weight were least affected by FA treatment and showed no statistically significant difference in comparison to WT (Figure S4D).

***Sprtn* silencing increases Tdp1 expression in zebrafish embryos and human cell**

To investigate the interplay between TDP1 and SPRTN at the gene expression level, we quantified their gene expressions under different conditions of gene silencing and DPC induction. In zebrafish

embryos, knockdown of *sprtn* resulted in a strong 2.2-fold increase in Tdp1 expression (Figure 6D), whereas this induction was much weaker in RPE1 cells where *Sprtn* silencing increased TDP1 expression by 1.2-fold (Figure 6A).
Brief acute exposure of embryos to CPT (10 µM, 1h) which strongly induced TOP1-DPCs (2.8-fold) (Figures 8A and 8B) resulted in a 29% (0.7-fold) decrease in Tdp1 expression (Figure 6D). In contrast, a lower dose of CPT (1 h, 10 nM) in RPE1 cells, which induced TOP1-DPCs by 4-fold (Figure 8E and F), did not significantly alter TDP1 expression (Figure 6A). The combination of *Sprtn* silencing and CPT treatment had no further effect on *tdp1* expression compared to *sprtn*-silenced non-treated embryos (Figure 6D). In contrast to the effects caused by CPT, treatment of WT embryos with FA (30 min, 5 mM) increased *tdp1* expression by 1.7-fold (Figure 6D). This effect was even more pronounced in FA-treated *sprtn*-silenced embryos, in which a 3.5-fold increase in *tdp1* expression was observed (Figure 6C).
The expression levels of *sprtn* in embryos were similar in WT and mutant embryos and did not change significantly after CPT exposure. However, FA increased *sprtn* expression 1.5-fold and 1.8-fold in WT and *tdp1* mutant embryos, respectively (Figure 6E). In RPE1 cells, *Tdp1* silencing caused a 10% decrease in *sprtn* expression (Figure 6B), whereas CPT exposure increased *Sprtn* expression by 1.2-fold (Figure 6B). Silencing and knockdown efficiencies are shown in Figures S3 and S4A, respectively.

Tdp2 **expression increases in Tdp1-deficient RPE1 cells and zebrafish embryos**

In the absence of TDP1, TDP2 can participate in the Top1-mediated DNA damage in cultured DT40 cells and *in vitro* (Zeng et al., 2012; Ledesma,2009). Therefore, we wanted to determine whether *Tdp2* expression increases when *Tdp1* is depleted in cells and embryos. In RPE1 cells, *Tdp2* expression remains the same under physiological conditions after silencing *Tdp1* or *Sprtn*. However, when cells are treated with CPT (10 nM, 1 h), a TOP1-DPC inducer, TDP2 expression increases strongly (1.8-fold) in *Tdp1*-silenced cells and moderately (1.3-fold) in *Sprtn*-silenced cells (Figure 6C). These data suggest that TDP2 may help overcome camptothecin-induced DNA damage in the absence of TDP1 in human cells. Because zebrafish has two *tdp2* orthologs, *tdp2a* (gene ID: 101887157) and *tdp2b* (gene ID: 553516), we performed qPCR analysis for both genes. In the absence of Tdp1, the expression of both genes increased significantly: *tdp2a* by 3.7-fold and *tdp2b* by 1.6-fold (Figures 6F and G). Expression of *Tdp2a* also increased after Sprtn knockdown, by 1.6-fold in WT and 2.3-fold in *tdp1* mutants. The effect of *sprtn* silencing on *tdp2b* expression is similar to the pattern observed for *tdp2a*, with a 1.4-fold increase in WT and a 2.1-fold increase in *tdp1* mutants (Figure 6G). In contrast, the expression pattern of the two *tdp2* orthologs in *tdp1* mutants is different: silencing of *sprtn* in mutants strongly decreased *tdp2a* expression compared with nonsilenced mutants (Figure 6F), whereas the pattern is reverse with respect to *tdp2b* expression, where silencing of *sprtn* causes an increase in *tdp2b* mRNA levels (Figure 6G).

Tdp1 and Sprtn deficiency decreases cell viability

We observed a significant reduction in cell density after silencing of *Tdp1* and *Sprtn* in RPE1 cells, so we quantified this effect using the MTT assay. Considering that TDP2 could compensate for the loss of TDP1 (Ledesma et al., 2009), we also investigated the effects of TDP2 silencing in combination with the lack of TDP1 and SPRTN on cell survival. Individual silencing of TDP1, TDP2, or SPRTN decreased cell viability by 50% (Figure 7). Simultaneous silencing of TDP1 and SPRTN further decreased cell viability by 68% ($p < 0.0001$). Interestingly, the effect was most pronounced when both TDP1 and TDP2 were silenced and viability decreased by 80%. We observed a similar effect, an 84% decrease in viability, after all three genes were silenced (Figure 7). The experiment was performed three times (biological triplicates), and silencing efficiencies were measured for each condition (Figure S5).

Tdp1 repairs Top1- and histone H3-DPCs *in vivo*

DPC isolates were analysed for the presence of TOP1- and histone H3-DPCs by Western blot or dot-blot using protein-specific antibodies. Four biological replicates were used for detection of TOP1- and H3- DPCs in zebrafish embryos, whereas three biological replicates were used for detection in RPE1 cells. Tdp1-deficient embryos exhibit greatly increased Top1-DPC levels under physiological conditions (4.8-fold more than WT) (Figures 8A and 8B). In comparison, the effect of the TOP1-DPC inducer, CPT (10 µM, 1 hour) was weaker in WT embryos: 2.6-fold increase compared to WT (Figure 8A and B). CPT further increased Top1-DPC levels in *tdp1* mutants (6.2-fold) (Figure 8A and B). FA treatment (5 mM, 30 min) had a much stronger effect on Top1-DPC induction than CPT in both, WT, and mutant embryos: FA induced Top1-DPC levels by 7.1-fold in WT and by 9-fold in *tdp1* mutant embryos (Figure 8A and B).
In RPE1 cells, the pattern of TOP1-DPC induction was to some extent similar to that in embryos. TOP1-DPCs accumulated strongly in RPE1 cells after *Tdp1* silencing (3.7-fold increase) (Figures 8E and S6A). In comparison, CPT, a TOP1-DPC inducer, caused a 2.2-fold increase in WT cells (Figures 8E and 8F). When cells were further challenged by the combination of TDP1 deficiency and CPT, TOP1-DPC levels increased 7.1-fold compared to nontreated WT cells (Figure 8F), confirming that TDP1 is critical for TOP1-DPC removal in cell culture. In comparison, FA treatment (1 mM, 20 min) had a very strong effect on TOP1- DPC increase in WT cells, and this induction did not increase further in the background of single or double gene silencing (Figures 8G and 8H).
To investigate whether TDP1 is involved in the repair of DPCs other than TOP1-DPCs, we chose to examine histones as possible TDP1 substrates based on the recent *in vitro* data of Wei et al. (2022), who showed that purified TDP1 removes crosslinked H4 and H2B at abasic sites. We chose histone H3 as a representative of the core histones because we had optimized protocols and a very sensitive antibody for its detection in the DPC isolates. In the embryos, the lack of Tdp1 led to a very strong accumulation of endogenous H3-DPCs: a 4.2-fold increase compared with WT embryos (Figures 9A and 9B). This is a very similar increase to that we observed for the canonical substrate of Tdp1, Top1-DPC, in *tdp1* mutants (4.8-fold) (Figures 8A and 8B). CPT treatment caused a 4.7-fold H3 DPC increase in WT and even greater increase of 7.3-fold in *tdp1* mutants (Figures 9A and 9B), consistent with a pattern similar to that observed for Top1 DPC accumulation after CPT exposure (Figure 8A and B). The FA treatment had a similar effect in WT and *tdp1* mutant embryos, namely a 5.3- and 5.1-fold increase in H3-DPCs (Figure 9 C and D).
In RPE1 cells, *Tdp1* silencing induced H3-DPC levels by 2.5-fold compared with untreated WT cells. It is important to note that CPT, although previously known to be a specific TOP1-DPC inducer, increased H3-DPCs 2.9-fold in WT cells (Figure 9E and F and S6 B and C). H3-DPC levels were comparably affected when WT or *Tdp1*-silenced cells were exposed to CPT: 2.9-fold and 2.8-fold increase, respectively (Figures 9E, 9F, S6B and S6C). In contrast, CPT induced many more H3-DPCs in *tdp1* mutants (7.3-fold), then in CPT-treated WT embryos (4.6-fold increase) (Figures 9A and 9B). FA caused a remarkable 15.7-fold increase in H3-DPCs in WT cells and a 25.8-fold increase in *Tdp1*-silenced cells compared with WT untreated cells (Figures 9D and 9G).

SPRTN proteolysis is necessary for TOP1 and H3 DPC repair *in vivo*

To test the hypothesis that upstream proteolysis by SPRTN is required for the subsequent action of TDP1 in removing TOP1-DPC, we measured TOP1-DPC levels in embryos and cells under different conditions. In WT embryos, knockdown of *sprtn* caused a 3.5-fold increase in Top1-DPCs levels (Figures 8C and 8D). In *tdp1* mutant embryos, the increase in Top1-DPCs before and after *sprtn* knockdown was similar, 3.5 and 4.7-fold, respectively (Figures 8C, 8D and S6A). Surprisingly, CPT treatment (10 µM, 1 hour) did not result in an additional increase in Top1-DPC levels in *sprtn*-silenced embryos (with functional Tdp1) (Figure 8C and 8D). Compared with untreated WT embryos, CPT exposure of embryos deficient in both Tdp1 and Sprtn increased Top1-DPC levels 6.9-fold, representing a significant

increase in Top1-DPC levels compared with *tdp1* mutants or *sprtn*-silenced mutants (Figures 8C and 8D). FA treatment (5mM, 30 min) of *sprtn*-silenced embryos with functional Tdp1 caused a significant 5.8-fold increase in Top1-DPC levels compared with untreated WT embryos, representing a significant increase compared with untreated *sprtn*-silenced embryos (3.5-fold). In sprtn-silenced tdp1 mutants, exposure with FA significantly increased TOP1 DPC levels compared with nontreated sprtn-silenced *tdp1* mutants ($p < 0.005$) (Figures 8C and 8D).
In RPE1 cells, silencing of *Sprtn* resulted in a large increase in TOP1-DPC levels (3.6-fold), a similar effect to silencing of *Tdp1* (3.65-fold) (Figures 8E and 8F). When both *Sprtn* and *Tdp1* were silenced, TOP1-DPCs accumulated dramatically (14.3-fold increase), suggesting that both proteins are involved in TOP1-DPCs removal. The same setup after CPT exposure (10 nM, 1h) showed a different pattern: *Sprtn* silencing caused a 12.6-fold increase, *Tdp1* silencing 7.1-fold increase, whereas double silencing additionally increased TOP1-DPC levels by 29.2-fold (Figures 8E and F). FA treatment (1 mM, 20 min) dramatically increased TOP1-DPC levels to a similar extent under all conditions (Figures 8G and H).
In embryos, *sprtn* knockdown had a tremendous effect on H3-DPC levels in both, WT and *tdp1* mutants with 5.7- and 5.1-fold increase, respectively (Figures 9A and B). CPT (10 µM, 1 hour) caused a different pattern of H3-DPC induction in the same backgrounds: a 4.8-fold increase in *sprtn*-silenced embryos and a 6.6-fold increase in *sprtn*-silenced *tdp1* mutants. Both inductions were weaker than in CPT-treated mutant embryos with functional Sprtn (7.3-fold) (Figures 9A and 9B). The levels of H3-DPCs observed in *tdp1* mutants after exposure to CPT show a significant increase compared to the endogenous levels of H3-DPCs in *tdp1* mutants ($P < 0.0001$). Moreover, this increase is even greater than the increase caused by *sprtn* silencing in *tdp1* mutants ($P < 0.0001$) (Figures 9A and B). At the same time, H3-DPC levels were similarly induced after *sprtn* silencing in WT and mutant embryos before and after CPT treatment (Figures 9 G and H). Compared with CPT-treated WT or *tdp1* mutant embryos, knockdown of *sprtn* had no further effect on the increase in H3-DPCs ($p < 0.05$) (Figure 9 A and B). *Sprtn* knockdown in FA-treated embryos (5 mM, 30 min) further increased H3-DPC levels compared with embryos with functional Sprtn: 8- and 8.5-fold increases in WT and mutants, respectively, versus 5.3- and 5.1-fold increases in WT and mutants with functional Sprtn, respectively (Figures 9C and D).
In RPE1 cells, SPRTN deficiency caused a very strong accumulation of H3-DPCs (3.2-fold increase) (Figures 9E, 9F, S6B and S6C). No additional effects on H3-DPC levels were observed when both *Sprtn* and *Tdp1* were silenced. *Sprtn* silencing in untreated and in CPT-treated cells increased H3-DPCs similarly: by 3.2- and 3.2-fold, respectively (Figures 9E and 9F). However, simultaneous silencing of *Tdp1* and *Sprtn*, followed by exposure to CPT had an additive effect on H3-DPC levels resulting in a 7.9-fold increase (Figure 9E, 9F, S6B and S6C). This increase is not as strong as for TOP1-DPC levels, where CPT treatment after simultaneous silencing dramatically increased TOP1-DPCs: from 14.3-fold to 29.2-fold (Figures 8E and 8F). When exposed to FA (1 mM, 20 min), *Sprtn*-silenced cells, as well as *Sprtn*- and *Tdp1*- silenced cells exhibited a 1.8- and 1.9-fold increases in H3-DPCs, respectively, compared with FA-treated WT cells (Figures 9G and 9H).

Discussion

Using the Tdp1-deficient zebrafish strain and RPE1 cells, we show that TDP1 is a key factor for repair of histone H3- and TOP1-DPCs, while SPRTN is crucial for the repair of multiple cellular DPCs and specific TOP1- and H3-DPCs. We show that H3-DNA crosslink resolution is dependent on upstream proteolysis by SPRTN and subsequent peptide removal by TDP1 in cells and embryos. In contrast to H3-DPC repair, where SPRTN and TDP1 function together, we show that they work in separate pathways during repair of endogenous TOP1-DPCs.
To study DPC repair *in vivo*, we first needed to establish the toolbox for using the zebrafish animal model in DPC research, which included DPC isolation and detection protocols from embryonic tissues (Materials and Methods, 2.7), generation of a Tdp1-deficient zebrafish strain, morpholino-mediated *sprtn* knockdown, and zebrafish Tdp1 antibody. Second, we analysed the degree of conservation of

TDP1 between humans and zebrafish and found that zebrafish is an acceptable vertebrate model for studying TDP1 function. The high degree of evolutionary conservation of the one-to-one orthology of TDP1 across all domains of life (Figure 1B) and the very high structural similarity between zebrafish and human orthologs (Figure 1A) indicate the importance of TDP1 in DNA repair during evolution.
Very high mRNA expression levels of *Tdp1* and *Sprtn* during embryonic development indicate that both repair factors are critical in the developing embryo (Figure 3A), which is not surprising given the very high rate of cell division and transcription and the high requirement for precise DNA repair (Keller, 2013). Tdp1 is highly expressed in human testis (Uhlén et al., 2015) and zebrafish and mouse gonads (Figure 3B and C), suggesting its protective role in germ cells. A similar mRNA tissue expression pattern of *Tdp1* in zebrafish and laboratory mouse (Figure 3B and C) indicates that zebrafish may be a good model for future investigation of the tissue-specific function of TDP1 in DPCR. Comparison with human expression data is currently not possible because the mRNA expression dataset available in the Human protein Atlas is heavily biased toward analysis of older individuals (Uhlén et al., 2015).
We observed that loss of Tdp1 in zebrafish embryos and RPE1 cells results in a significant increase in medium- and high-molecular weight DPCs that cannot be attributed to the increase in H3- and TOP1-DPCs (Figure 4 and 5), suggesting that TDP1 has multiple DPC substrates. On the other hand, the increase in low molecular weight DPCs in *tdp1* mutant embryos and TDP1-deficient RPE1 cells (Figure 4C and 5C) is most likely due to the increase in histone-DPCs, considering that endogenous H3 DPCs accumulate strongly in Tdp1-deficient embryos and cells (Figure 9). Our data support the recent observations of Wei *et al.* (2022), who showed that TDP1 can remove histone H2B and H4 from AP sites *in vitro*, and provide evidence for a novel, TDP1-dependent repair pathway for histone-DPCs *in vivo*. The function of TDP1 in the repair of cellular DPCs and histone-DPCs has not been previously investigated and our results should be taken into account when considering the development of TDP1 inhibitors in cancer therapy (Sun et al., 2020).
With respect to the known TDP1 substrate TOP1, we found that TDP1 is indeed crucial for the removal of TOP1-DPCs, both at the organism level and in RPE1 cells (Figure 8). As expected, silencing of *Tdp1* in RPE1 cells increased TOP1-DPC levels (Figure 8E) similar to HEK293 human cells (Fielden et al., 2020). Many studies have investigated the role of TDP1 in TOP1-DPCs removal *in vitro* and in cell lines (Gao et al., 2014; Heidrun & James, 2011; Pouliot et al., 1999; Yang et al., 1996), but data on the vertebrate model were lacking (Hirano et al., 2007; Katyal et al., 2007). Here, we show that Tdp1 deficiency in zebrafish embryos leads to a significant 4.2-fold increase in endogenous TOP1-DPCs (Figure 8A). Our results are in contrast to the observations of Zaksauskaite *et al.* (2021), who found no difference in TOP1-DPC levels between wild-type and Tdp1-deficient zebrafish embryos. The discrepancy is likely due to the different approaches to DPC isolation, as the RADAR assay is more specific and sensitive than the CsCl fractionation method used in the previous study (Kiianitsa & Maizels, 2013, 2014, 2020). Detailed insights into the repair of TOP1-DPCs at the organism level are of importance to biomedicine, as TOP1 inhibitors, camptotecin derivatives irinotecan and topotecan, which act as TOP1-DPC inducers, are used to treat various cancers including ovarian and colon cancer, small-cell lung cancer, central nervous system tumours, and sarcomas (Martino et al., 2017). Combination therapies with TOP1 and TDP1 inhibitors could significantly improve current clinical protocols, and thus it is important to understand how TDP1 functions in DPCR at the organism level.
With respect to the SPRTN protease, we show that it is a crucial protease for the resolution of multiple cellular DPCs *in vivo*, particularly low- and medium- molecular weight DPCs (Figures 4 and 5). By analysing DPCs in SPRTN-deficient embryos, we provide the first evidence of how DPC levels are affected in an organism. Compared with embryos, the effect of SPRTN deficiency was somewhat weaker in RPE1 cells, but this is consistent with previous reports (Fielden et al., 2020). Our results also show that SPRTN plays an important role in the resolution of H3-DPCs *in vivo*, as knockdown of *sprtn* in zebrafish resulted in a 5.7-fold increase in H3-DPC levels (Figure 9A and B), supporting *in vitro* data that showed that H3 is a substrate of SPRTN (Vaz et al., 2016). We also demonstrated that SPRTN is crucial for TOP1-DPC repair *in vivo* (Figure 8A and B), supporting previous studies in cells that showed that TOP1-DPC levels increase after SPRTN silencing (Maskey et al., 2017; Stingele et al., 2014a; Vaz et

al., 2016) and that SPRTN proteolyzes TOP1 *in vitro* (Vaz et al., 2016). Therefore, our study finally demonstrates the crucial role of SPRTN in resolving DPCs *in vivo* and highlights SPRTN as a promising new chemotherapeutic target.

Regarding the interaction of TDP1 and SPRTN in DPCR under physiological conditions, SPRTN and TDP1 are known to play distinct roles in DPC repair. SPRTN is required for initiating repair of many crosslinked proteins (Fielden et al., 2018), whereas TDP1 has been specifically associated with repair of TOP1-DPCs (Kawale & Povirk, 2018). Indeed, our results in RPE1 cells suggest a non-epistatic relationship between these two proteins in the repair of total cellular DPCs (Figure 5A and B). However, we show that they work together in the resolution of endogenous H3-DPCs in embryos and RPE1 cells (Figures 9A, 9B, 9E and 9F), suggesting that SPRTN is the main protease acting upstream of TDP1-mediated peptide removal in the resolution of histone-DPCs at AP sites. These results confirm the hypothesis of Pachva *et al.* (2020) that SPRTN proteolysis is required for histone-DPC resolution. However, it is worth noting that TDP1 can remove H2B and H4 crosslinks *in vitro* without requiring upstream proteolysis (Wei et al., 2022). It is very important to understand how histone-DPCs are repaired due to their high frequency under physiological conditions. More than 10,000 abasic sites are generated daily (Lindahl, 1993), and about 10% of these lead to the formation of DPCs, most of which are histone-DPCs (Kiianitsa & Maizels, 2020). This suggests that hundreds, possibly even thousands of histones are cross-linked daily to abasic sites in each individual cell (Ren et al., 2019).

Surprisingly, our data suggest that TDP1 and SPRTN function in parallel (nonepistatically) during repair of endogenous TOP1-DPCs in RPE1 cells (Figure 8E and F). We observed a similar pattern in embryos, but the changes were not statistically significant in this case because of higher variability between experiments (Figure 8C and D). Since it is known that TDP1 cannot process TOP1-DPCs alone (Heidrun & James, 2011), we hypothesise that another protease is involved in the upstream proteolysis of endogenous TOP1-DPCs. Possible candidates include DDI1, DDI2, FAM111A, and the proteasome (Dirac-Svejstrup et al., 2020; Kojima et al., 2020; Larsen et al., 2019; Serbyn et al., 2020). The interplay between SPRTN and TDP1 is also evident at the level of mRNA expression, where silencing of SPRTN increases TDP1 expression in both embryos and cells (Figure 6A and D). Both proteins are critical for normal cell function, as RPE1 cells with silenced TDP1 and SPRTN exhibit a 68% reduction in viability (Figure 7). We suggest that this phenotype is the result of impaired DPCR resulting from the absence of TDP1 and SPRTN (Figure 4, 5, 8 and 9), as SPRTN-silenced human cells exit S phase with abnormal replication intermediates (Mórocz et al., 2017) and TDP1-silenced cells exhibit an increase in ssDNA and dsDNA breaks (Fielden et al., 2020).

In contrast to physiological conditions, after CPT exposure, when TOP1-DPCs are induced, we show that SPRTN and TDP1 act epistatically in resolving total DPCs in RPE1 cells (Figure 5A, B, D and E). Our results are consistent with data from cell survival assays showing that simultaneous depletion of TDP1 and SPRTN in yeast (Stingele *et al.*, 2014; Lopez-Mosqueda *et al.*, 2016) and HeLa cells (Vaz et al., 2016) causes hypersensitivity to CPT treatment to a similar extent as depletion of either component alone suggesting that SPRTN and TDP1 function in the same pathway during exposure to CPT. Therefore, it is important to note that DPCR factors may behave differently under physiological conditions and under stress. In summary, our results suggest that, unlike repair of endogenous TOP1-DPCs, in which TDP1 and SPRTN function in separate pathways, repair of CPT-induced TOP1-DPCs in cells relies on the SPRTN-TDP1 pathway. It is important to note that CPT also induces H3-DPCs in human cells and in zebrafish embryos (Figures 9, S6B and S6C), demonstrating for the first time that CPT is not specific for TOP1-DPC induction, as previously thought (Ramawat & Mérillon, 2013). Moreover, expression analysis of Tdp2 showed a significant increase in Tdp2 when Tdp1 was absent in embryos suggesting that Tdp2 may compensate for loss of Tdp1 *in vivo*, supporting previous observations from cell culture and in vitro experiments (Ledesma et al., 2009; Zeng et al., 2012).

Formaldehyde is a potent crosslinker of various cellular proteins ranging in size from 10 kDa to over 200 kDa (Stingele *et al.*, 2014; Lopez-Mosqueda *et al.*, 2016; Ruggiano *et al.*, 2021). Our results show that the interplay of SPRTN and TDP1 in DPCR is altered when cells and embryos are exposed to high acute doses of FA, compared with physiological conditions in which only endogenous DPCs are

present. SPRTN and TDP1 act together (in epistasis) in the repair of FA-induced total cellular DPCs (Figure 4 and 5G and H) and H3- and TOP1- DPCs (Figure 8 and 9). Considering that large amounts of DPCs accumulate under these conditions, we hypothesise that SPRTN is fully activated and performs upstream proteolysis of many cross-linked proteins given its pleiotropic nature (Vaz et al., 2016), and that TDP1 is crucial for the resolution of H3- and TOP1-DPCs along with any additional damage of a similar nature at the ssDNA breaks.
In summary, we performed a comprehensive analysis of the role of TDP1 and SPRTN in DPC resolution in zebrafish embryos and human RPE1 cells. Our results reveal the interplay of these proteins in the resolution of cellular DPCs, H3- and TOP1-DPCs and introduce a novel TDP1-mediated repair pathway for histone-DPCs that highlights the epistatic relationship between upstream SPRTN proteolysis and downstream TDP1 3' DNA end processing. Furthermore, we demonstrate the essential role of both proteins in the resolution of total cellular DPCs and TOP1-DPCs in cells and embryos. These results provide important insights into complex DPC repair pathways and their implications for human disease and cancer treatments. Further research in this area will advance our understanding of DPC repair pathways and their potential therapeutic applications.

Figure legends

Figure 1. Structural, phylogenetic and syntenic comparison of TDP1 in zebrafish, human, and mouse. A) The zebrafish Tdp1 structural model (in green) is overlapped with the human TDP1 crystal structure (PDB: 1jy1) (Davies et al., 2002), shown in grey (N domain) and black (C domain). Zebrafish Tdp1 was modelled using the Phyre2 workspace (Kelley et al., 2015) according to the human TDP1 (PDB: c1nopB). N domain and C domain form a pseudo-2-fold axis, of symmetry where each domain contributes to the active site: H263, K265 and N283 in the N domain and H493, K495 and N516 in the C domain. B) Phylogenetic analysis of TDP1 proteins. The vertebrate TDP1 cluster is shown in dark green, invertebrate cluster, which is phylogenetically closely related to vertebrate orthologs, is shown in light green, second invertebrate cluster is shown in blue. Plant and algae clusters are shown in dark and light red, respectively, while fungi and bacterial orthologs are shown in dark and light grey, respectively. C) Synteny analysis between the zebrafish, human, and mouse *tdp1* gene were made using Genomicus (Louis et al., 2013). The numbers next to the gene names represent the megabase pair (Mbp) of each gene position on the chromosome.

Figure 2. Validation and characterization of the zebrafish *tdp1* mutant line. A) Amino acid sequence of Tdp1 in *tdp1* mutant fish line: frameshift and introduction of a premature stop codon in *tdp1* mutant fish line is deduced from DNA sequencing (*, premature STOP). B) TDP1 activity assay was performed on 600 ng of lysate from 2-dpf WT and *tdp1* mutant embryos. On the left, scheme of the substrate displays two forms that are generated after TDP1 activity. 5' end of the oligonucleotide has attached Cy5 which serves as a fluorescent reporter and 3' end has attached tyrosine (pY). After TDP1 activity, the tyrosine residue is removed, leaving a 3' end phosphate group (p). C) Western blot using a custom antibody against zebrafish Tdp1 shows the absence of a specific Tdp1 signal (68 kDa, indicated by arrow) in *tdp1* mutant embryo lysate. Histon H3 was used as a loading control. D) Images of WT and *tdp1* mutant embryos (2dpf, 2 days post fertilization) and adult fish (6 months old). Embryos were maintained in E3 media, placed on a lid of a 96-well culture plate, and visualized with stereo microscope (Motic-SMZ-171-TP). Prior to imaging, adult fish were anesthetized with tricaine methanesulfonate or MS -222 (0.02% in aquarium water) for 10 minutes. Images were captured using a Canon 250D DSLR camera.

Figure 3. Tdp1 expression profiles in zebrafish embryos and zebrafish and mouse adults A) Tdp1 and Sprtn expression patterns during the embryonic development from 6 hours post fertilization (6 hpf) to 5 days post fertilization (5 dpf). Data represent MNE (mean normalized expression) ± SD (n = 3) normalized to the housekeeping gene Atp50 B) Tissue expression pattern of Tdp1 in male and female

zebrafish, with statistically significant differences between expression in ovaries and testes (*$P < 0.05$) determined by unpaired t-test. Data are presented as MNE (mean normalized expression) ± SD (n = 3) normalized to the housekeeping gene Atp50 (C) Tissue expression pattern of Tdp1 in male and female mice (ns, non significant, $P > 0.05$). Data represents MNE (mean normalized expression) ± SD (n = 3) normalized to the housekeeping gene Atp50.

Figure 4. DPC analysis in Tdp1 and/or Sprtn deficient embryos before and after CPT (10 µM, 1h) and FA (5 mM, 30 min) treatment. A) DPCs were isolated from 2 dpf embryos using the RADAR assay (30 embryos per condition, n = 4), resolved on the SDS acrylamide gel, and stained with silver (left panel - low exposure, right panel - high exposure). Dot-blots showing DNA loading controls for DPC analysis prior to bensonase treatment are shown below (A DPC equivalent of 200 ng total DNA was loaded per well). DPCs were analysed as total and according to size where LMW are below 40 kDa, MMW 40 kDa to 150 kDa, and HMW above 150 kDa. B) Quantification of A. Quantifications of LMW (C), MMW (D) and HMW (E) from (A). Data represent mean fold change to WT ± SD (n = 4), statistical significance was established using an unpaired Student's t-test (*($P < 0.05$), **($P < 0.01$), ***($P < 0.001$), and ****($P < 0.0001$)).

Figure 5. DPC analysis in RPE1 cells after *tdp1* and *sprtn* gene silencing before and after CPT (10 nM, 1h) and FA (1 mM, 20 min) treatment. Silencing was carried out for 72 hours prior to collection, and the efficiency of each condition was confirmed using QPCR (Figures S4A). A) Total DPC levels after gene silencing and DNA loading controls below the silver-stained gels B) and C) Quantification of total, LMW, MMW and HMW DPCs normalized to non-treated WT cells from four independent experiments (n = 4) D) Total DPC levels after CPT exposure dot-blots showing DNA loading controls for DPC analysis prior to bensonase treatment are shown below E) Quantification of D (n = 3) F) CPT shows the greatest effect on LMW DPCs (quantification from D). G) Total DPC levels after FA exposure with DNA loading controls. H) Quantification of G (n = 3). Samples were normalized to WT. I) A strong increase is observed in LMW and MMW DPC levels in FA-treated cells. All conditions were normalized to WT and statistical analysis was performed with GraphPad Prism software using an unpaired t-test (*($P < 0.05$), **($P < 0.01$), ***($P < 0.001$), or ****($P < 0.0001$)).

Figure 6. SPRTN, TDP1 and 2 expression levels following *tdp1* and *sprtn* gene silencing in RPE1 cells and Sprtn knockdown in WT and *tdp1* mutant embryos. A) Expression levels of TDP1 in RPE1 cells after SPRTN silencing and after CPT exposure (50 nM, 1 hour) B) SPRTN levels decrease after TDP1 silencing and increase after CPT exposure. C) TDP2 significantly increases after TDP1 silencing and exposure to CPT. D) Zebrafish Tdp1 expression levels significantly increase in embryos after Sprtn knockdown. E) No significant change in Sprtn expression was detected between WT and the *tdp1* mutant before and after CPT treatment. F) Tdp2a expression is significantly increased in *tdp1* mutants before and after Sprtn silencing and in WTs after Sprtn silencing. (G) Tdp2b expression significantly increased in *tdp1* mutants before and after Sprtn silencing and in WTs after Sprtn silencing. Results are presented as fold changes to WT (mean ± SD) from four biological replicates. Unpaired t-tests were performed with GraphPad Prism, with significant shown as * ($P < 0.05$), **($P < 0.01$), ***($P < 0.001$), or ****($P < 0.0001$)

Figure 7. Cell viability after TDP1, SPRTN and/or TDP2 silencing in RPE1 cells. All measurements were normalized to WT from three different experiments. Corresponding silencing efficiencies are shown in supplementary Figure S5. (mean ± SD; n = 3 independent experiments; ****$P < 0.0001$, unpaired Student's t-test)

Figure 8. Tdp1 deficiency causes strong accumulation of endogenous and chemically induced TOP1 DPCs in embryos and cells. (A) Western blot showing zebrafish Top 1 DPCs in *tdp1* mutant embryos before and after CPT (10 µM, 1 hour) and FA treatment (5mM, 30 min) (DPC equivalent of 1 µg DNA was loaded per well) and (B) corresponding quantification (n = 4). (C) Western blot showing zebrafish

Top 1 DPCs in *tdp1* mutant embryos before and after Sprtn silencing and CPT (10 µM, 1 hour) and FA treatment (5mM, 30 min) and (D) corresponding quantification. E) Dot blots showing TOP1 DPCs detected with TOP1-specific antibody before and after CPT treatment (10 nM, 1 hour) with corresponding DNA loading controls (DPC equivalent of 500 ng DNA was loaded per well). Cells were treated with 10 nM CPT for 1 hour. F) Quantification of A from three different biological replicates normalised to untreated WT cells. G) Dot blots showing TOP1 DPCs detected with TOP1-specific antibody before and after FA treatment (1 mM, 20 min) with corresponding DNA loading controls (DPC equivalent of 500 ng DNA was loaded per well). H) Quantification of C (n = 3). Results represent mean fold change ± SD of three different experiments. Statistically significant changes as a result from unpaired Student's t-test are shown as * ($P < 0.05$), **($P < 0.01$), *** ($P < 0.001$) or **** ($P < 0.0001$).

Figure 9. H3 DPC levels are increased *in vivo* in *tdp1* mutant fish line and in RPE cells with TDP1 deficiency. A) Western blot showing H3 DPC levels in *tdp1* mutant embryos in combination with Sprtn knockdown and CPT (10 µM, 1h) treatment. Total DPCs were isolated from 2-day old embryos, separated by SDS-PAGE (DPC equivalent of 200 ng DNA per well) and detected with H3-specific antibody. B) Quantifications of H3 DPCs from four biological replicates with mean (± SD) fold change to endogenous WT H3 DPCs levels. C) Western blot analysis of H3 DPCs in zebrafish embryos and (D) corresponding quantification after FA treatment (1 mM for 20 min) (n = 4). E) Dot blots showing H3 DPCs after silencing TDP1 and/or SPRTN before and after CPT exposure (10 nM CPT, 1h) and DNA loading controls. Equivalent of 200 ng DNA of total DPCs was loaded per sample. (F) Quantification of H3 DPC analysis (n = 3). G) Dot blots showing H3 DPCs after silencing TDP1 and/or SPRTN before and after FA exposure (1 mM FA, 20 min) and DNA loading controls and H) Corresponding quantification (n = 3). Results are presented as mean ± SD with statistically significant changes, determined using an unpaired Student's t-test are indicated with *($P < 0.05$), **($P < 0.01$), ***($P < 0.001$), and ****($P < 0.0001$).

Supplementary Figure legends

Figure S1. (A) Extended phylogenetic analysis of TDP1 proteins from bacteria to humans. The vertebrate TDP1 cluster is shown in dark green, invertebrate cluster, which is phylogenetically closely related to vertebrate orthologs, is shown in light green, second invertebrate cluster is shown in blue. Plant and algae clusters are shown in dark and light red, respectively, while fungi and bacterial orthologs are shown in dark and light grey, respectively. **(B)** The plot of disorder disposition for zebrafish Tdp1 protein predicted by PONDR-FIT software. Values above 0.5 indicate likely disordered regions (N-terminal), while structured N- and C-domains are labelled in grey and yellow, respectively.

Figure S2. DNA sequencing *tdp1* mutant line and verification of newly developed Tdp1 antibody which recognizes both, zebrafish and human protein (A) Sequencing od *tdp1* mutant fish line that contains allele 1 with change; insertion of CTT after 1510 and two substitutions of A1512 to G and G1515 to A was selected in male fish, and allele 2; five nucleotide insertion after position 1512 (TAAAA), and G 1513 substitution to A was selected in female F1 fish. Both of this change result in premature stop at amino acid position 44 of zebrafish Tdp1. B) Western blot showing that custom-made Tdp1 antibody recognizes the overexpressed human TDP1 recombinant protein in HEK293 cells. Histone H3 is shown as a loading control.

Figure S3. Knockdown efficiency of Sprtn morpholino in zebrafish embryos. A) DNA gel electrophoresis showing the resolution of PCR reactions performed on cDNA isolated from two-day-old embryos after injection of exon-skipping morpholino into one cell stage embryos and primers listed in Table 3. B) Sprtn silencing efficiency was approximated as a reduction in WT bend, quantified by Image J and presented as a fold change to WT (mean ± SD) (n = 4).

Figure S4. Silencing efficiencies and DPCs analyses in RPE1 cells. A) Efficiency of TDP1 and SPRTN silencing in RPE1 cells. Cells were incubated with siRNAs listed in Table 1 for 72 hours. The success of silencing was approximated by qPCR, and the results are shown as the mean percent reduction in expression to untreated WT cells ± SD (n = 9). B) Higher exposure to silver staining of total DPCs following gene silencing of Figure 5A with DNA loading controls below the silver-stained gel. C) Quantification of MMW and HMW DPCs from Figure 5D normalized to non-treated WT (mean ± SD; n = 3 independent experiments; *($P < 0.05$), **($P < 0.01$), ***($P < 0.001$), unpaired Student t-test), D) Quantification of high molecular size proteins after exposure to FA from Figure 5G.

Figure S5. TDP1, SPRTN, and TDP2 silencing efficiencies for the MTT cell viability assay. In parallel with the seeding of cells for the MTT viability assay shown in Figure 7, cells were seeded for silencing verification using the same experimental conditions. Silencing efficiencies are approximated using qPCR analysis and presented as the percentage reduction in expression to WT ± SD from three technical replicates.

Figure S6. DPC analysis for Top1 and H3 DPCs which were used as biological replicates for the quantifications in Figures 8D and 9F. A) Western blot showing zebrafish Top 1 DPCs in *tdp1* mutant embryos before and after silencing of Sprtn and treatment with CPT (10 µM, 1 hour) and FA (5mM, 30 min). B) and C) display dot blot analyses of H3 DPCs from two additional experiments after silencing TDP1 and/or SPRTN, and following exposure to CPT (10 nM CPT, 1h), along with DNA loading controls. In experiments, the equivalent of 200 ng DNA of total DPCs was loaded per sample.

References

Abràmoff, M. D., Magalhães, P. J., & Ram, S. J. (2004). Image processing with imageJ. *Biophotonics International*, *11*(7), 36–41. https://doi.org/10.1201/9781420005615.ax4

Anisimova, M., & Gascuel, O. (2006). Approximate likelihood-ratio test for branches: A fast, accurate, and powerful alternative. *Systematic Biology*, *55*(4), 539–552. https://doi.org/10.1080/10635150600755453

Bradford, Y. M., Van Slyke, C. E., Ruzicka, L., Singer, A., Eagle, A., Fashena, D., Howe, D. G., Frazer, K., Martin, R., Paddock, H., Pich, C., Ramachandran, S., & Westerfield, M. (2022). Zebrafish information network, the knowledgebase for Danio rerio research. *Genetics*, *220*(4). https://doi.org/10.1093/genetics/iyac016

Chesner, L. N., & Campbell, C. (2018). A quantitative PCR-based assay reveals that nucleotide excision repair plays a predominant role in the removal of DNA-protein crosslinks from plasmids transfected into mammalian cells. *DNA Repair*, *62*(October 2017), 18–27. https://doi.org/10.1016/j.dnarep.2018.01.004

Choi, T. Y., Choi, T. I., Lee, Y. R., Choe, S. K., & Kim, C. H. (2021). Zebrafish as an animal model for biomedical research. *Experimental and Molecular Medicine*, *53*(3), 310–317. https://doi.org/10.1038/s12276-021-00571-5

Davies, D. R., Interthal, H., Champoux, J. J., & Hol, W. G. J. (2002). The crystal structure of human tyrosyl-DNA phosphodiesterase, Tdp1. *Structure*, *10*(2), 237–248. https://doi.org/10.1016/S0969-2126(02)00707-4

Deng, C., Brown, J. A., You, D., & Brown, J. M. (2005). Multiple endonucleases function to repair covalent topoisomerase I complexes in Saccharomyces cerevisiae. *Genetics*, *170*(2), 591–600. https://doi.org/10.1534/genetics.104.028795

Dirac-Svejstrup, A. B., Walker, J., Faull, P., Encheva, V., Akimov, V., Puglia, M., Perkins, D., Kümper, S., Hunjan, S. S., Blagoev, B., Snijders, A. P., Powell, D. J., & Svejstrup, J. Q. (2020). DDI2 Is a Ubiquitin-Directed Endoprotease Responsible for Cleavage of Transcription Factor NRF1. *Molecular Cell*, *79*(2), 332-341.e7. https://doi.org/10.1016/j.molcel.2020.05.035

Duxin, J. P., Dewar, J. M., Yardimci, H., & Walter, J. C. (2014). Repair of a DNA-protein crosslink by replication-coupled proteolysis. *Cell*, *159*(2), 346–357. https://doi.org/10.1016/j.cell.2014.09.024

Fengzhi Li, T. J. Q. L. X. L. (2017). Camptothecin analogues and their molecular targets. *Am J Cancer Res*, *7*(12), 2350–2394. https://www.ncbi.nlm.nih.gov/pmc/articles/PMC5752681/

Fielden, J., Ruggiano, A., Popović, M., & Ramadan, K. (2018). DNA protein crosslink proteolysis repair: From yeast to premature ageing and cancer in humans. *DNA Repair*, *71*(August), 198–204. https://doi.org/10.1016/j.dnarep.2018.08.025

Fielden, J., Wiseman, K., Torrecilla, I., Li, S., Hume, S., Chiang, S. C., Ruggiano, A., Narayan Singh, A., Freire, R., Hassanieh, S., Domingo, E., Vendrell, I., Fischer, R., Kessler, B. M., Maughan, T. S., El-Khamisy, S. F., & Ramadan, K. (2020). TEX264 coordinates p97- and SPRTN-mediated resolution of topoisomerase 1-DNA adducts. *Nature Communications*, *11*(1), 1–16. https://doi.org/10.1038/s41467-020-15000-w

Gao, R., Das, B. B., Chatterjee, R., Abaan, O. D., Agama, K., Matuo, R., Vinson, C., Meltzer, P. S., & Pommier, Y. (2014). Epigenetic and genetic inactivation of tyrosyl-DNA-phosphodiesterase 1 (TDP1) in human lung cancer cells from the NCI-60 panel. *DNA Repair*, *13*(1), 1–9. https://doi.org/10.1016/j.dnarep.2013.09.001

Guindon, S., & Gascuel, O. (2003). A Simple, Fast, and Accurate Algorithm to Estimate Large Phylogenies by Maximum Likelihood. *Systematic Biology*, *52*(5), 696–704. https://doi.org/10.1080/10635150390235520

Heidrun, I., & James, J. (2011). effects of DNA and protein size on substrate cleavage by human tyrosyl-DNA phosphodiesterase 1 (TDP1). *Biochemical Journal*, *436*(3), 559–566. https://doi.org/10.1042/BJ20101841.Effects

Hirano, R., Interthal, H., Huang, C., Nakamura, T., Deguchi, K., Choi, K., Bhattacharjee, M. B., Arimura, K., Umehara, F., Izumo, S., Northrop, J. L., Salih, M. A. M., Inoue, K., Armstrong, D. L., Champoux, J. J., Takashima, H., & Boerkoel, C. F. (2007). Spinocerebellar ataxia with axonal neuropathy: Consequence of a Tdp1 recessive neomorphic mutation? *EMBO Journal*, *26*(22), 4732–4743. https://doi.org/10.1038/sj.emboj.7601885

Interthal, H., Chen, H. J., & Champoux, J. J. (2005). Human Tdp1 cleaves a broad spectrum of substrates, including phosphoamide linkages. *Journal of Biological Chemistry*, *280*(43), 36518–36528. https://doi.org/10.1074/jbc.M508898200

Katoh, K., Misawa, K., Kuma, K. I., & Miyata, T. (2002). MAFFT: A novel method for rapid multiple sequence alignment based on fast Fourier transform. *Nucleic Acids Research*, *30*(14), 3059–3066. https://doi.org/10.1093/nar/gkf436

Katyal, S., El-Khamisy, S. F., Russell, H. R., Li, Y., Ju, L., Caldecott, K. W., & McKinnon, P. J. (2007). TDP1 facilitates chromosomal single-strand break repair in neurons and is neuroprotective in vivo. *EMBO Journal*, *26*(22), 4720–4731. https://doi.org/10.1038/sj.emboj.7601869

Kawale, A. S., & Povirk, L. F. (2018). Tyrosyl-DNA phosphodiesterases: Rescuing the genome from the risks of relaxation. *Nucleic Acids Research*, *46*(2), 520–537. https://doi.org/10.1093/nar/gkx1219

Keller, P. J. (2013). In vivo imaging of zebrafish embryogenesis. *Methods*, *62*(3), 268–278. https://doi.org/10.1016/j.ymeth.2013.03.015

Kelley, L. A., Mezulis, S., Yates, C. M., Wass, M. N., & Sternberg, M. J. (2015). The Phyre2 web portal for protein modeling, prediction and analysis. *Nature Protocols*, *10*(6), 845–858. https://doi.org/10.1038/nprot.2015-053

Kiianitsa, K., & Maizels, N. (2013). A rapid and sensitive assay for DNA-protein covalent complexes in living cells. *Nucleic Acids Research*, *41*(9), 1–7. https://doi.org/10.1093/nar/gkt171

Kiianitsa, K., & Maizels, N. (2014). Ultrasensitive isolation, identification and quantification of DNA-protein adducts by ELISA-based RADAR assay. *Nucleic Acids Research*, *42*(13), 1–12. https://doi.org/10.1093/nar/gku490

Kiianitsa, K., & Maizels, N. (2020). The “adductome”: A limited repertoire of adducted proteins in human cells. *DNA Repair*, *89*(December 2019), 102825. https://doi.org/10.1016/j.dnarep.2020.102825

Kojima, Y., Machida, Y., Palani, S., Caulfield, T. R., Radisky, E. S., Kaufmann, S. H., & Machida, Y. J. (2020). FAM111A protects replication forks from protein obstacles via its trypsin-like domain. *Nature Communications*, *11*(1). https://doi.org/10.1038/s41467-020-15170-7

Laev, S. S., Salakhutdinov, N. F., & Lavrik, O. I. (2016). Tyrosyl-DNA phosphodiesterase inhibitors: Progress and potential. *Bioorganic and Medicinal Chemistry*, *24*(21), 5017–5027. https://doi.org/10.1016/j.bmc.2016.09.045

Larsen, N. B., Gao, A. O., Sparks, J. L., Gallina, I., Wu, R. A., Mann, M., Räschle, M., Walter, J. C., & Duxin, J. P. (2019). Replication-Coupled DNA-Protein Crosslink Repair by SPRTN and the Proteasome in Xenopus Egg Extracts. *Molecular Cell*, *73*(3), 574-588.e7. https://doi.org/10.1016/j.molcel.2018.11.024

Ledesma, F. C., El Khamisy, S. F., Zuma, M. C., Osborn, K., & Caldecott, K. W. (2009). A human 5’-tyrosyl DNA phosphodiesterase that repairs topoisomerase-mediated DNA damage. *Nature*, *461*(7264), 674–678. https://doi.org/10.1038/nature08444

Lessel, D., Vaz, B., Halder, S., Lockhart, P. J., Marinovic-Terzic, I., Lopez-Mosqueda, J., Philipp, M., Sim, J. C. H., Smith, K. R., Oehler, J., Cabrera, E., Freire, R., Pope, K., Nahid, A., Norris, F., Leventer, R. J., Delatycki, M. B., Barbi, G., Von Ameln, S., … Kubisch, C. (2014). Mutations in SPRTN cause early onset hepatocellular carcinoma, genomic instability and progeroid features. *Nature Genetics*, *46*(11), 1239–1244. https://doi.org/10.1038/ng.3103

Lin, C. P., Ban, Y., Lyu, Y. L., Desai, S. D., & Liu, L. F. (2008). A ubiquitin-proteasome pathway for the repair of topoisomerase I-DNA covalent complexes. *Journal of Biological Chemistry*, *283*(30), 21074–21083. https://doi.org/10.1074/jbc.M803493200

Lin, C. Y., Chiang, C. Y., & Tsai, H. J. (2016). Zebrafish and Medaka: New model organisms for modern biomedical research. *Journal of Biomedical Science*, *23*(1), 1–11. https://doi.org/10.1186/s12929-016-0236-5

Liu, C., Pouliot, J. J., & Nash, H. A. (2002). Repair of topoisomerase I covalent complexes in the absence of the tyrosyl-DNA phosphodiesterase Tdp1. *Proceedings of the National Academy of Sciences of the United States of America*, *99*(23), 14970–14975. https://doi.org/10.1073/pnas.182557199

Lončar, J., Popović, M., Krznar, P., Zaja, R., & Smital, T. (2016). The first characterization of multidrug and toxin extrusion (MATE/SLC47) proteins in zebrafish (Danio rerio). *Scientific Reports*, *6*(June), 1–15. https://doi.org/10.1038/srep28937

Lopez-Mosqueda, J., Maddi, K., Prgomet, S., Kalayil, S., Marinovic-Terzic, I., Terzic, J., & Dikic, I. (2016). SPRTN is a mammalian DNA-binding metalloprotease that resolves DNA-protein crosslinks. *ELife*, *5*(NOVEMBER2016), 1–19. https://doi.org/10.7554/eLife.21491

Louis, A., Muffato, M., & Crollius, H. R. (2013). Genomicus: Five genome browsers for comparative genomics in eukaryota. *Nucleic Acids Research*, *41*(D1), 700–705. https://doi.org/10.1093/nar/gks1156

Martino, E., Della Volpe, S., Terribile, E., Benetti, E., Sakaj, M., Centamore, A., Sala, A., & Collina, S. (2017). The long story of camptothecin: From traditional medicine to drugs. *Bioorganic and Medicinal Chemistry Letters*, *27*(4), 701–707. https://doi.org/10.1016/j.bmcl.2016.12.085

Maskey, R. S., Flatten, K. S., Sieben, C. J., Peterson, K. L., Baker, D. J., Nam, H. J., Kim, M. S., Smyrk, T. C., Kojima, Y., Machida, Y., Santiago, A., Van Deursen, J. M., Kaufmann, S. H., & Machida, Y. J. (2017). Spartan deficiency causes accumulation of Topoisomerase 1 cleavage complexes and tumorigenesis. *Nucleic Acids Research*, *45*(8), 4564–4576. https://doi.org/10.1093/nar/gkx107

Mathavan, S., Lee, S. G. P., Mak, A., Miller, L. D., Murthy, K. R. K., Govindarajan, K. R., Tong, Y., Wu, Y. L., Lam, S. H., Yang, H., Ruan, Y., Korzh, V., Gong, Z., Liu, E. T., & Lufkin, T. (2005). Transcriptome analysis of zebrafish embryogenesis using microarrays. *PLoS Genetics*, *1*(2), 0260–0276. https://doi.org/10.1371/journal.pgen.0010029

Modzelewski, A. J., Chen, S., Willis, B. J., Lloyd, K. C. K., Joshua, A., & He, L. (2018). *RNP Electroporation of Zygotes) technology*. *13*(6), 1253–1274. https://doi.org/10.1038/nprot.2018.012.Efficient

Moreno-Mateos, M. A., Vejnar, C. E., Beaudoin, J. D., Fernandez, J. P., Mis, E. K., Khokha, M. K., & Giraldez, A. J. (2015). CRISPRscan: Designing highly efficient sgRNAs for CRISPR-Cas9 targeting in vivo. *Nature Methods*, *12*(10), 982–988. https://doi.org/10.1038/nmeth.3543

Mórocz, M., Zsigmond, E., Tóth, R., Zs Enyedi, M., Pintér, L., & Haracska, L. (2017). DNA-dependent protease activity of human Spartan facilitates replication of DNA-protein crosslink-containing DNA. *Nucleic Acids Research*, *45*(6), 3172–3188. https://doi.org/10.1093/nar/gkw1315

Muller, P. Y., Janovjak, H., Miserez, A. R., & Dobbie, Z. (2002). Processing of gene expression data generated by quantitative real-time RT-PCR. *BioTechniques*, *32*(6), 1372-1374,1376,1378-1379.

Nasevicius, A., & Ekker, S. C. (2000). Effective targeted gene “knockdown” in zebrafish [In Process Citation]. *Nat Genet*, *26*(2), 216–220.

Otten, C., Knox, J., Boulday, G., Eymery, M., Haniszewski, M., Neuenschwander, M., Radetzki, S., Vogt, I., Hähn, K., De Luca, C., Cardoso, C., Hamad, S., Igual Gil, C., Roy, P., Albiges-Rizo, C., Faurobert, E., Kries, J. P., Campillos, M., Tournier-Lasserve, E., … Abdelilah-Seyfried, S. (2018). Systematic pharmacological screens uncover novel pathways involved in cerebral cavernous

malformations. *EMBO Molecular Medicine*, *10*(10), 1–17. https://doi.org/10.15252/emmm.201809155

Pachva, M. C., Kisselev, A. F., Matkarimov, B. T., Saparbaev, M., & Groisman, R. (2020). DNA-Histone Cross-Links: Formation and Repair. *Frontiers in Cell and Developmental Biology*, *8*(December), 1–14. https://doi.org/10.3389/fcell.2020.607045

Penn, O., Privman, E., Ashkenazy, H., Landan, G., Graur, D., & Pupko, T. (2010). GUIDANCE: A web server for assessing alignment confidence scores. *Nucleic Acids Research*, *38*(SUPPL. 2), 23–28. https://doi.org/10.1093/nar/gkq443

Pommier, Y., Huang, S. yin N., Gao, R., Das, B. B., Murai, J., & Marchand, C. (2014). Tyrosyl-DNA-phosphodiesterases (TDP1 and TDP2). *DNA Repair*, *19*, 114–129. https://doi.org/10.1016/j.dnarep.2014.03.020

Pommier, Y., Nussenzweig, A., Takeda, S., & Austin, C. (2022). Human topoisomerases and their roles in genome stability and organization. *Nature Reviews Molecular Cell Biology*, *23*(6), 407–427. https://doi.org/10.1038/s41580-022-00452-3

Popovic, M., Zaja, R., Fent, K., & Smital, T. (2013). Molecular characterization of zebrafish Oatp1d1 (Slco1d1), a novel organic anion-transporting polypeptide. *Journal of Biological Chemistry*, *288*(47), 33894–33911. https://doi.org/10.1074/jbc.M113.518506

Pouliot, J. J., Yao, K. C., Robertson, C. A., & Nash, H. A. (1999). *Pouliot1999*. *286*(October).

Prasad, R., Horton, J. K., Dai, D. P., & Wilson, S. H. (2019). Repair pathway for PARP-1 DNA-protein crosslinks. *DNA Repair*, *73*(July 2018), 71–77. https://doi.org/10.1016/j.dnarep.2018.11.004

Ramawat, K. G., & Mérillon, J.-M. (2013). Natural Products: Phytochemistry, Botany and Metabolism of Alkaloids, Phenolics and Terpenes. *Natural Products*.

Ray Chaudhuri, A., Hashimoto, Y., Herrador, R., Neelsen, K. J., Fachinetti, D., Bermejo, R., Cocito, A., Costanzo, V., & Lopes, M. (2012). Topoisomerase i poisoning results in PARP-mediated replication fork reversal. *Nature Structural and Molecular Biology*, *19*(4), 417–423. https://doi.org/10.1038/nsmb.2258

Raymond, A. C., Rideout, M. C., Staker, B., Hjerrild, K., & Burgin, A. B. (2004). Analysis of human tyrosyl-DNA phosphodiesterase I catalytic residues. *Journal of Molecular Biology*, *338*(5), 895–906. https://doi.org/10.1016/j.jmb.2004.03.013

Reinking, H. K., Kang, H. S., Götz, M. J., Li, H. Y., Kieser, A., Zhao, S., Acampora, A. C., Weickert, P., Fessler, E., Jae, L. T., Sattler, M., & Stingele, J. (2020). DNA Structure-Specific Cleavage of DNA-Protein Crosslinks by the SPRTN Protease. *Molecular Cell*, *80*(1), 102-113.e6. https://doi.org/10.1016/j.molcel.2020.08.003

Ren, M., Bai, J., Xi, Z., & Zhou, C. (2019). DNA damage in nucleosomes. *Science China Chemistry*. https://doi.org/10.1007/s11426-018-9421-5

Ruggiano, A., & Ramadan, K. (2021a). DNA–protein crosslink proteases in genome stability. *Communications Biology*, *4*(1), 1–11. https://doi.org/10.1038/s42003-020-01539-3

Ruggiano, A., & Ramadan, K. (2021b). The Trinity of SPRTN Protease Regulation. *Trends in Biochemical Sciences*, *46*(1), 2–4. https://doi.org/10.1016/j.tibs.2020.10.007

Ruggiano, A., Vaz, B., Kilgas, S., Popović, M., Rodriguez-Berriguete, G., Singh, A. N., Higgins, G. S., Kiltie, A. E., & Ramadan, K. (2021). The protease SPRTN and SUMOylation coordinate DNA-protein crosslink repair to prevent genome instability. *Cell Reports*, *37*(10). https://doi.org/10.1016/j.celrep.2021.110080

Serbyn, N., Noireterre, A., Bagdiul, I., Plank, M., Michel, A. H., Loewith, R., Kornmann, B., & Stutz, F. (2020). The Aspartic Protease Ddi1 Contributes to DNA-Protein Crosslink Repair in Yeast. *Molecular Cell*, *77*(5), 1066-1079.e9. https://doi.org/10.1016/j.molcel.2019.12.007

Stingele, J., Bellelli, R., Alte, F., Hewitt, G., Sarek, G., Maslen, S. L., Tsutakawa, S. E., Borg, A., Kjær, S., Tainer, J. A., Skehel, J. M., Groll, M., & Boulton, S. J. (2016). Mechanism and Regulation of DNA-Protein Crosslink Repair by the DNA-Dependent Metalloprotease SPRTN. *Molecular Cell*, *64*(4), 688–703. https://doi.org/10.1016/j.molcel.2016.09.031

Stingele, J., Schwarz, M. S., Bloemeke, N., Wolf, P. G., & Jentsch, S. (2014a). A DNA-dependent protease involved in DNA-protein crosslink repair. *Cell*, *158*(2), 327–338. https://doi.org/10.1016/j.cell.2014.04.053

Stingele, J., Schwarz, M. S., Bloemeke, N., Wolf, P. G., & Jentsch, S. (2014b). A DNA-dependent protease involved in DNA-protein crosslink repair. *Cell*, *158*(2), 327–338. https://doi.org/10.1016/j.cell.2014.04.053

Sun, Y., Saha, S., Wang, W., Saha, L. K., Huang, S. Y. N., & Pommier, Y. (2020). Excision repair of topoisomerase DNA-protein crosslinks (TOP-DPC). *DNA Repair*, *89*(January), 102837. https://doi.org/10.1016/j.dnarep.2020.102837

Takashima, H., Boerkoel, C. F., John, J., Saifi, G. M., Salih, M. A. M., Armstrong, D., Mao, Y., Quiocho, F. A., Roa, B. B., Nakagawa, M., Stockton, D. W., & Lupski, J. R. (2002). Mutation of TDP1, encoding a topoisomerase I-dependent DNA damage repair enzyme, in spinocerebellar ataxia with axonal neuropathy. *Nature Genetics*, *32*(2), 267–272. https://doi.org/10.1038/ng987

Thomas S. Dexheimer, Smitha Antony, Christophe Marchand, and Y. P. (2008). Tyrosyl-DNA Phosphodiesterase as a Target for Anticancer Therapy. *Anticancer Agents Med Chem*, *23*(1), 1–7.

Tom, R., Bisson, L., & Durocher, Y. (2008). Transfection of adherent HEK293-EBNA1 cells in a six-well plate with branched PEI for production of recombinant proteins. *Cold Spring Harbor Protocols*, *3*(3). https://doi.org/10.1101/pdb.prot4978

Uhlén, M., Fagerberg, L., Hallström, B. M., Lindskog, C., Oksvold, P., Mardinoglu, A., Sivertsson, Å., Kampf, C., Sjöstedt, E., Asplund, A., Olsson, I. M., Edlund, K., Lundberg, E., Navani, S., Szigyarto, C. A. K., Odeberg, J., Djureinovic, D., Takanen, J. O., Hober, S., … Pontén, F. (2015). Tissue-based map of the human proteome. *Science*, *347*(6220). https://doi.org/10.1126/science.1260419

Vance, J. R., & Wilson, T. E. (2001). Repair of DNA Strand Breaks by the Overlapping Functions of Lesion-Specific and Non-Lesion-Specific DNA 3' Phosphatases. *Molecular and Cellular Biology*, *21*(21), 7191–7198. https://doi.org/10.1128/mcb.21.21.7191-7198.2001

Vance, J. R., & Wilson, T. E. (2002). Yeast Tdp1 and Rad1-Rad10 function as redundant pathways for repairing Top1 replicative damage. *Proceedings of the National Academy of Sciences of the United States of America*, *99*(21), 13669–13674. https://doi.org/10.1073/pnas.202242599

Vaz, B., Popovic, M., Newman, J. A., Fielden, J., Aitkenhead, H., Halder, S., Singh, A. N., Vendrell, I.,

Fischer, R., Torrecilla, I., Drobnitzky, N., Freire, R., Amor, D. J., Lockhart, P. J., Kessler, B. M., McKenna, G. W., Gileadi, O., & Ramadan, K. (2016). Metalloprotease SPRTN/DVC1 Orchestrates Replication-Coupled DNA-Protein Crosslink Repair. *Molecular Cell*, *64*(4), 704–719. https://doi.org/10.1016/j.molcel.2016.09.032

Vaz, B., Popovic, M., & Ramadan, K. (2017). DNA–Protein Crosslink Proteolysis Repair. *Trends in Biochemical Sciences*, *42*(6), 483–495. https://doi.org/10.1016/j.tibs.2017.03.005

Wang, P., Henning, S. M., & Heber, D. (2010). Limitations of MTT and MTS-based assays for measurement of antiproliferative activity of green tea polyphenols. *PLoS ONE*, *5*(4). https://doi.org/10.1371/journal.pone.0010202

Wei, X., Wang, Z., Hinson, C., & Yang, K. (2022). *3 -DNA – peptide / protein cross-links arising from abasic sites in vitro*. *50*(7), 1–20.

Xue, B., Dunbrack, R. L., Williams, R. W., Dunker, A. K., & Uversky, V. N. (2010). PONDR-FIT: A meta-predictor of intrinsically disordered amino acids. *Biochimica et Biophysica Acta - Proteins and Proteomics*, *1804*(4), 996–1010. https://doi.org/10.1016/j.bbapap.2010.01.011

Yang, S. W., Burgin, A. B., Huizenga, B. N., Robertson, C. A., Yao, K. C., & Nash, H. A. (1996). A eukaryotic enzyme that can disjoin dead-end covalent complexes between DNA and type I topoisomerases. *Proceedings of the National Academy of Sciences of the United States of America*, *93*(21), 11534–11539. https://doi.org/10.1073/pnas.93.21.11534

Zaksauskaite, R., Thomas, R. C., Van Eeden, F., & El-Khamisy, S. F. (2021). Tdp1 protects from topoisomerase 1-mediated chromosomal breaks in adult zebrafish but is dispensable during larval development. *Science Advances*, *7*(5), 1–16. https://doi.org/10.1126/SCIADV.ABC4165

Zeng, Z., Sharma, A., Ju, L., Murai, J., Umans, L., Vermeire, L., Pommier, Y., Takeda, S., Huylebroeck, D., Caldecott, K. W., & El-Khamisy, S. F. (2012). TDP2 promotes repair of topoisomerase I-mediated DNA damage in the absence of TDP1. *Nucleic Acids Research*, *40*(17), 8371–8380. https://doi.org/10.1093/nar/gks622

Figure 1

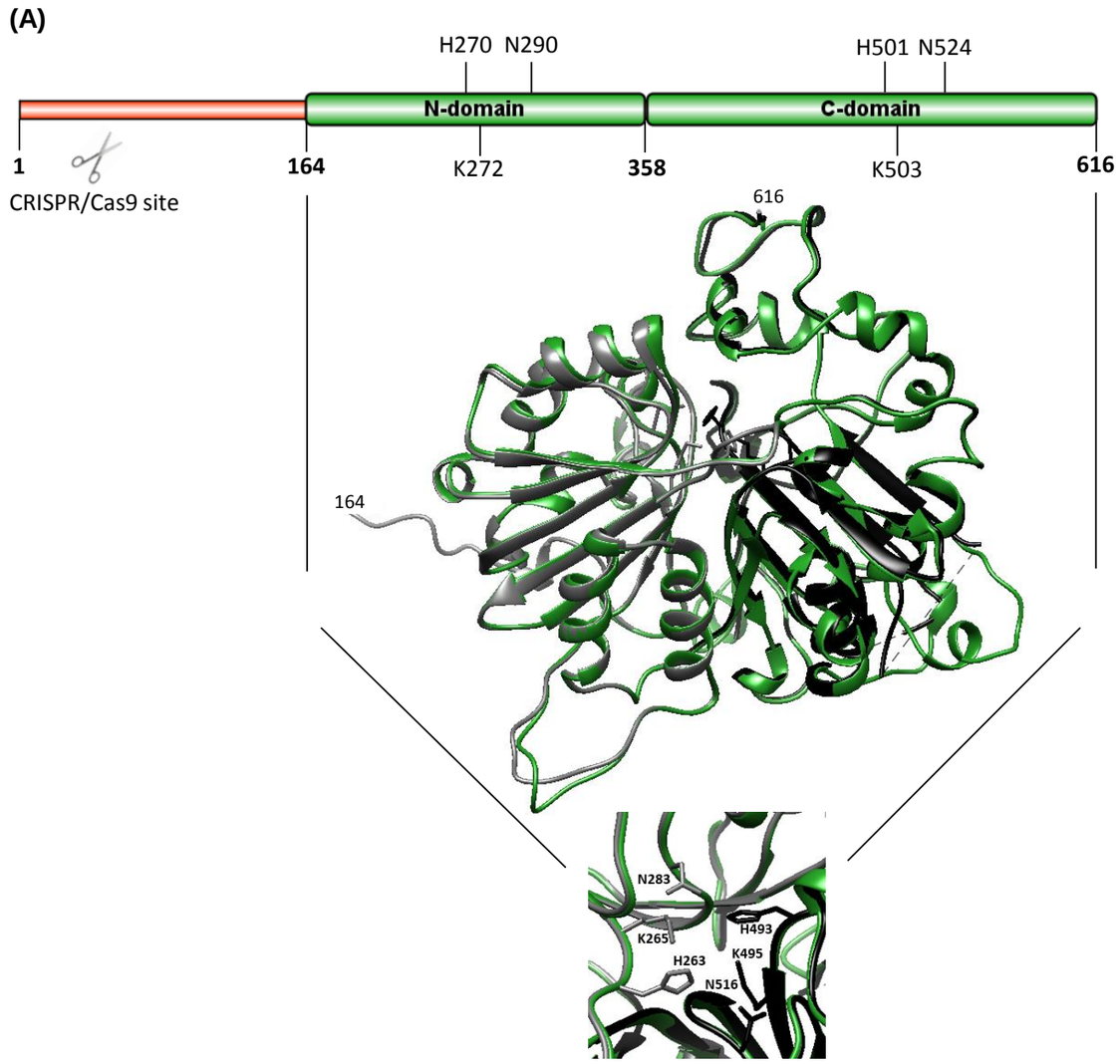
(A)
H270 N290
H501 N524
N-domain
C-domain
1
164
K272
358
K503
616
CRISPR/Cas9 site
616
164
N283
K265
H493
H263
K495
N516

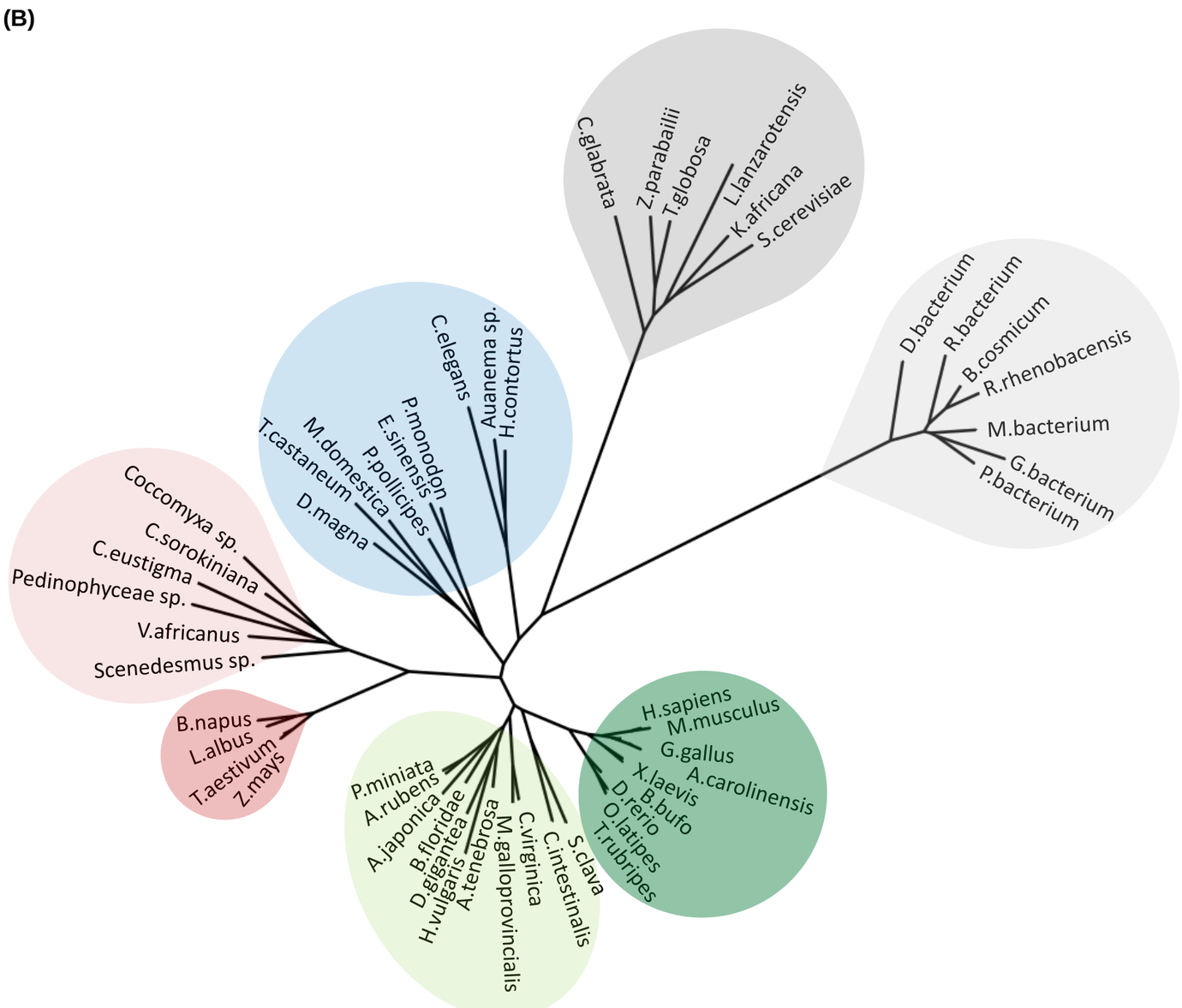
(B)
C.glabrata
Z.parabailii
T.globosa
L.lanzarotensis
K.africana
S.cerevisiae
C.elegans
Auanema sp.
H.contortus
P.monodon
E.sinensis
P.policipes
M.domestica
T.castaneum
D.magna
D.bacterium
R.bacterium
B.cosmicum
R.rhenobacensis
M.bacterium
G.bacterium
P.bacterium
Coccomyxa sp.
C.sorokiniana
C.eustigma
Pedinophyceae sp.
V.africanus
Scenedesmus sp.
B.napus
L.albus
T.aestivum
Z.mays
H.sapiens
M.musculus
G.gallus
A.carolinensis
X.laevis
B.bufo
D.rerio
O.latipes
T.rubripes
S.clava
C.intestinalis
C.virginica
M.galloprovincialis
A.tenebrosa
D.gigantea
B.floridae
H.vulgaris
A.japonica
A.rubens
P.miniata

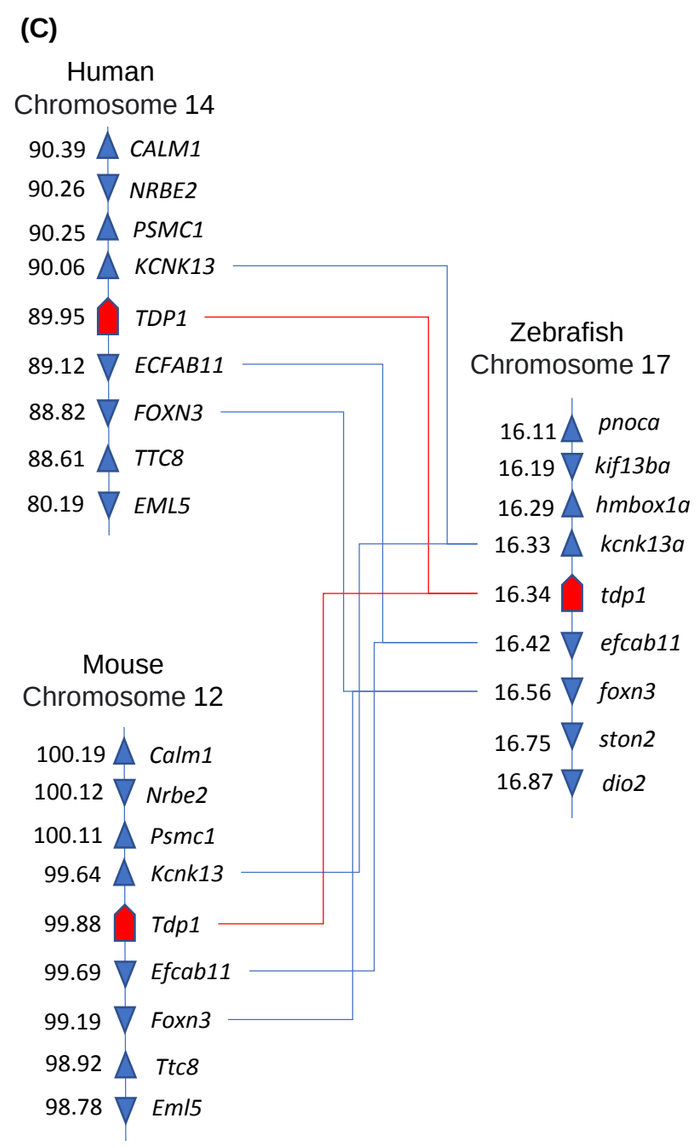
(C)
Human
Chromosome 14
90.39 CALM1
90.26 NRBE2
90.25 PSMC1
90.06 KCNK13
89.95 TDP1
89.12 ECFAB11
88.82 FOXN3
88.61 TTC8
80.19 EML5
Zebrafish
Chromosome 17
16.11 pnoca
16.19 kif13ba
16.29 hmbox1a
16.33 kcnk13a
16.34 tdp1
16.42 efcab11
16.56 foxn3
16.75 ston2
16.87 dio2
Mouse
Chromosome 12
100.19 Calm1
100.12 Nrbe2
100.11 Psmc1
99.64 Kcnk13
99.88 Tdp1
99.69 Efcab11
99.19 Foxn3
98.92 Ttc8
98.78 Eml5

Figure 2

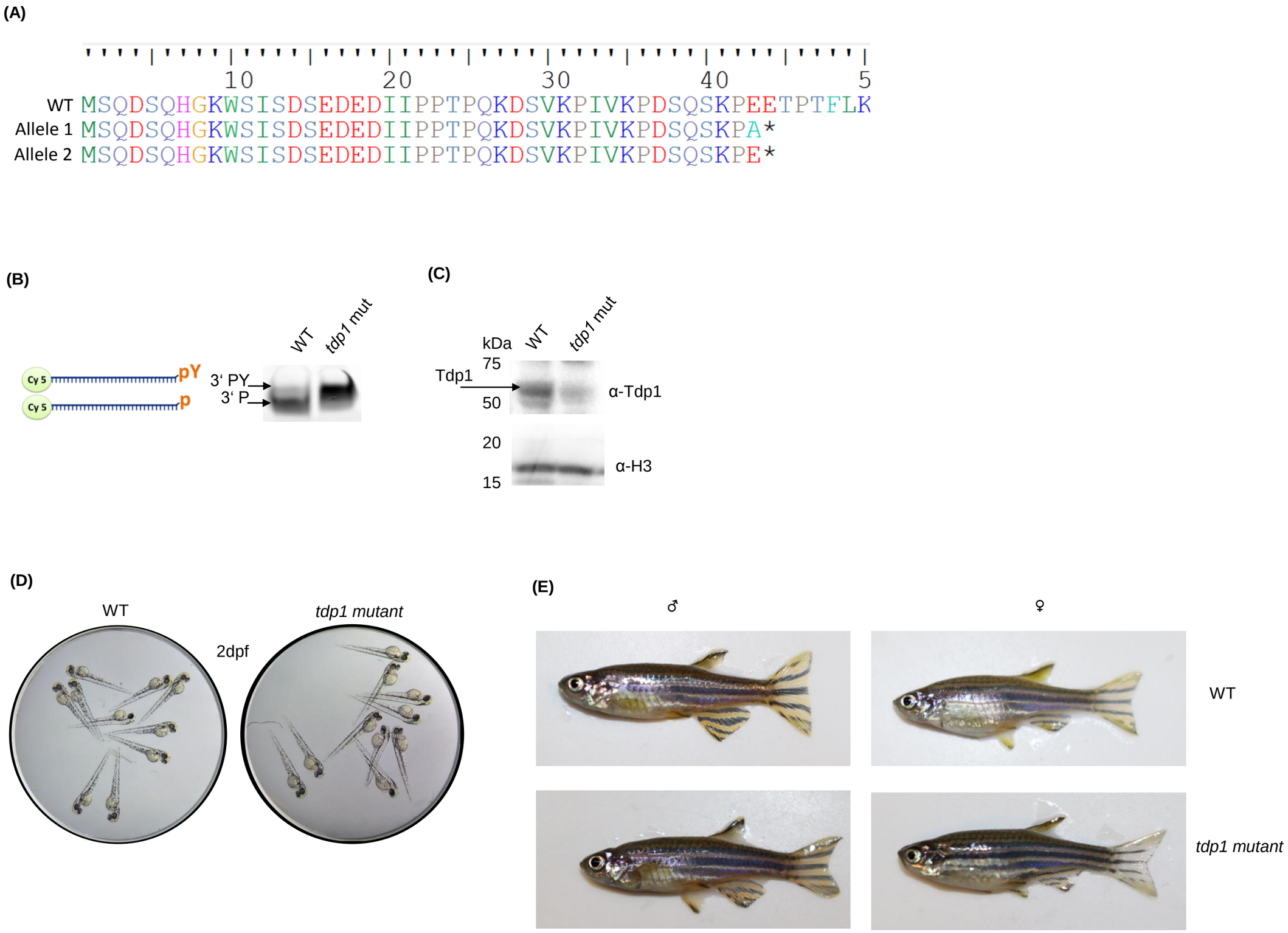
(A)
10
20
30
40
5
WT MSQDSQHGKWSISDSEDEDIIPPTPQKDSVKPIVKPDSQSKPEETPTFLK
Allele 1 MSQDSQHGKWSISDSEDEDIIPPTPQKDSVKPIVKPDSQSKPA*
Allele 2 MSQDSQHGKWSISDSEDEDIIPPTPQKDSVKPIVKPDSQSKPE*
(B)
Cy 5
pY
Cy 5
p
3‘ PY
3‘ P
WT
tdp1 mut
(C)
kDa
WT
tdp1 mut
75
Tdp1
50
α-Tdp1
20
α-H3
15
(D)
WT
tdp1 mutant
2dpf
(E)
♂
♀
WT
tdp1 mutant

Figure 3

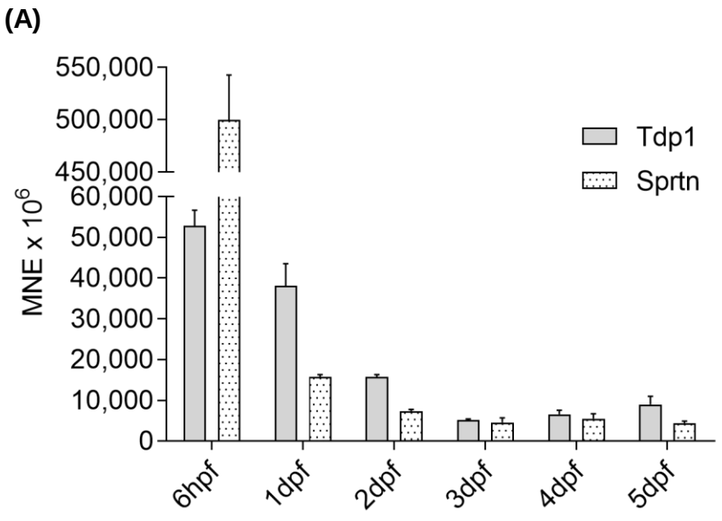
(A)
550,000
500,000
450,000
60,000
50,000
40,000
30,000
20,000
10,000
0
MNE x 10^6
Tdp1
Sprtn
6hpf
1dpf
2dpf
3dpf
4dpf
5dpf

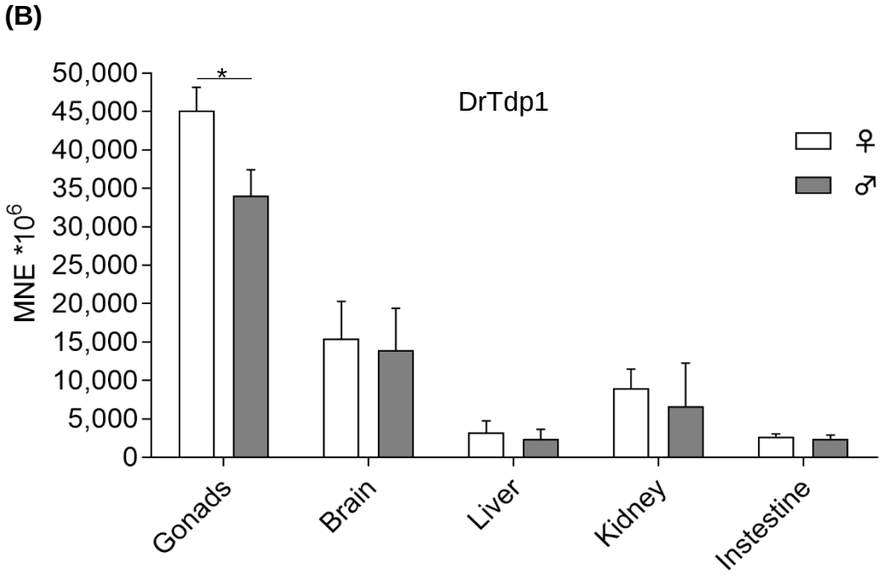
(B)
50,000
45,000
40,000
35,000
30,000
25,000
20,000
15,000
10,000
5,000
0
MNE *10^6
*
DrTdp1
♀
♂
Gonads
Brain
Liver
Kidney
Instestine

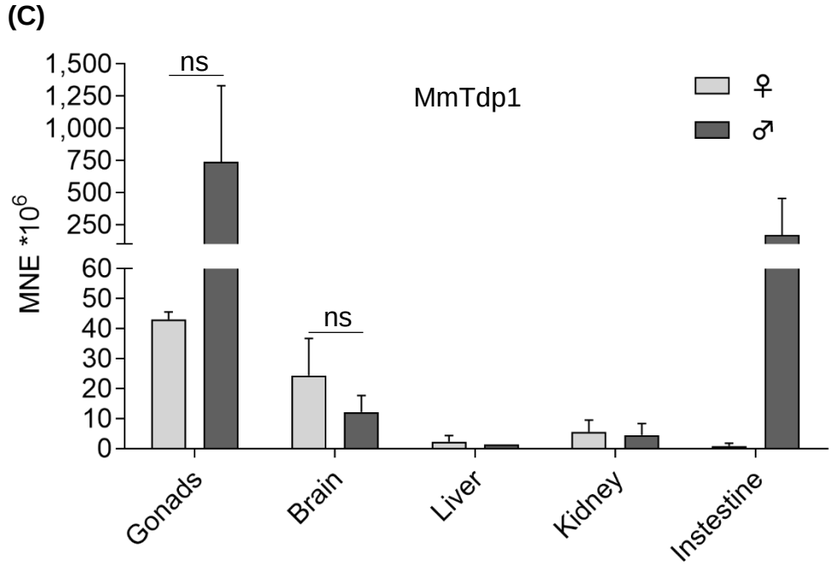
(C)
1,500
1,250
1,000
750
500
250
60
50
40
30
20
10
0
MNE *10^6
ns
ns
MmTdp1
♀
♂
Gonads
Brain
Liver
Kidney
Instestine

Figure 4

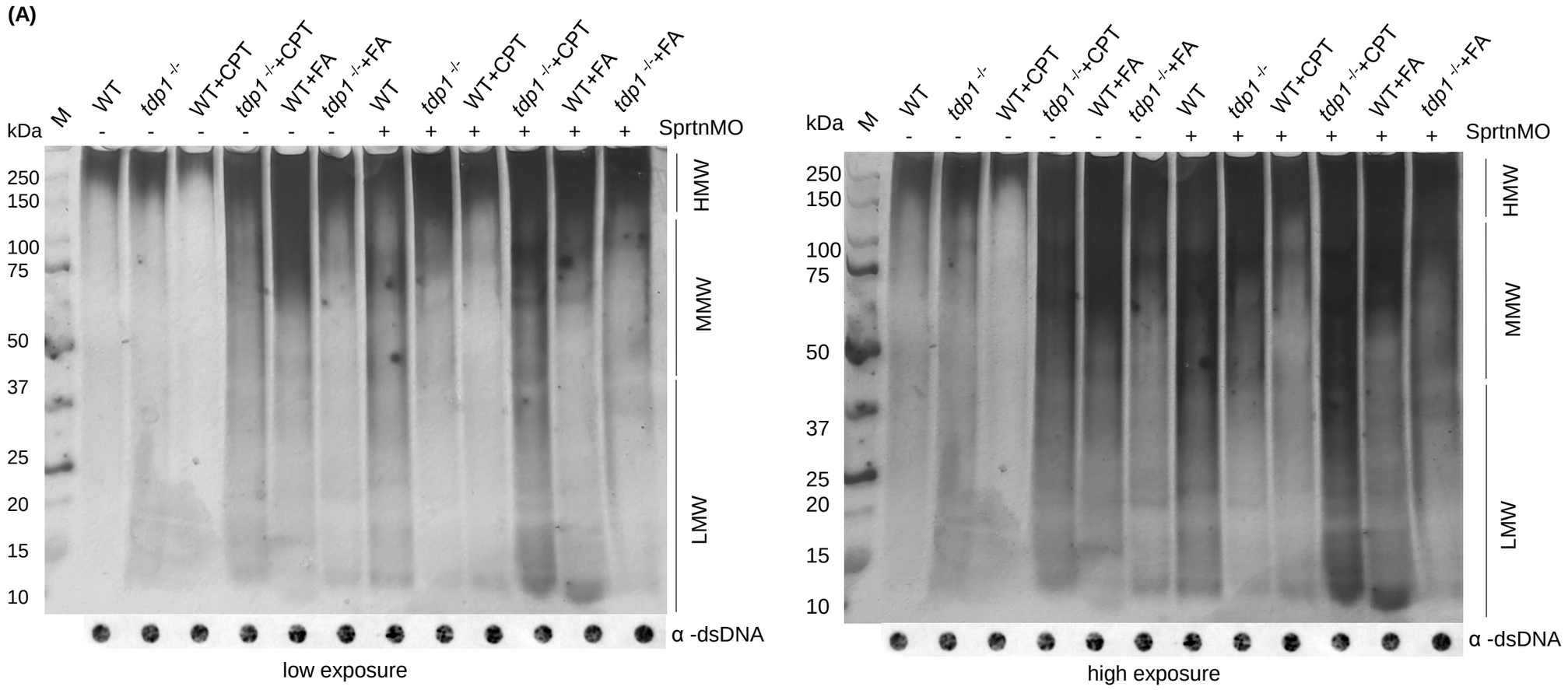
(A)
kDa
M
WT
tdp1 -/-
WT+CPT
tdp1 -/-+CPT
WT+FA
tdp1 -/-+FA
SprtnMO
250
150
100
75
50
37
25
20
15
10
HMW
MMW
LMW
α -dsDNA
low exposure
high exposure

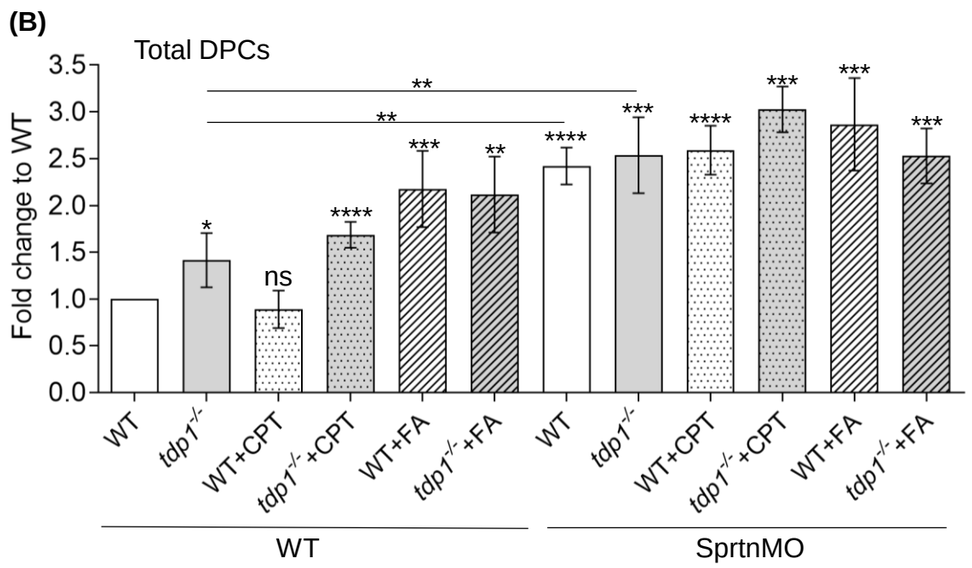
(B)
Total DPCs
Fold change to WT
WT
SprtnMO

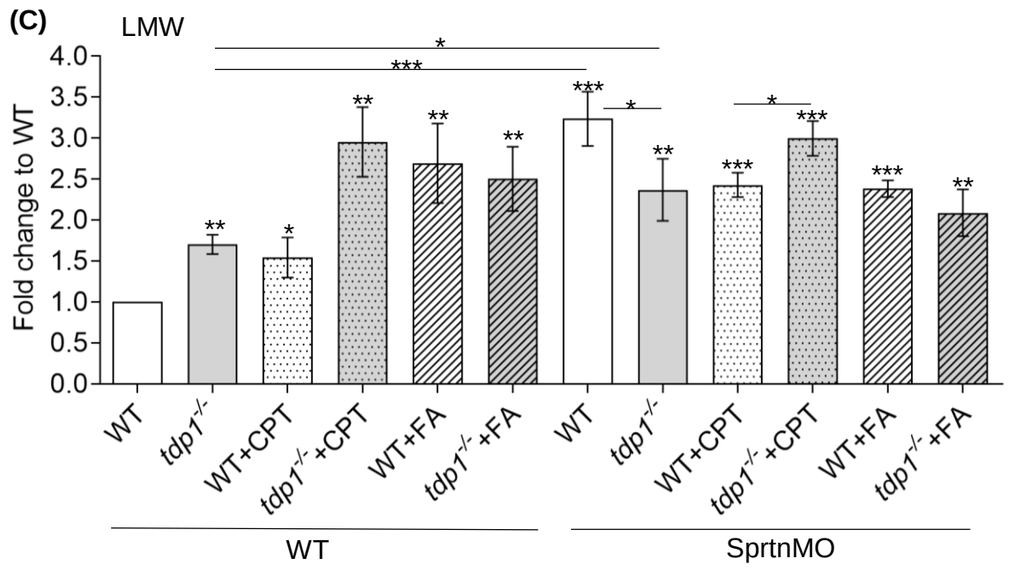
(C)
LMW
Fold change to WT
WT
SprtnMO

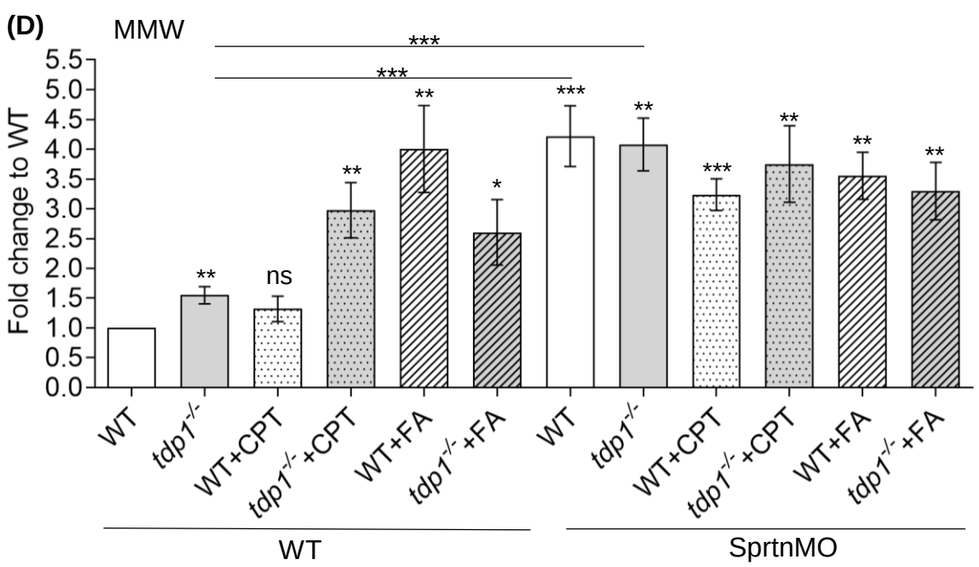
(D)
MMW
Fold change to WT
WT
SprtnMO

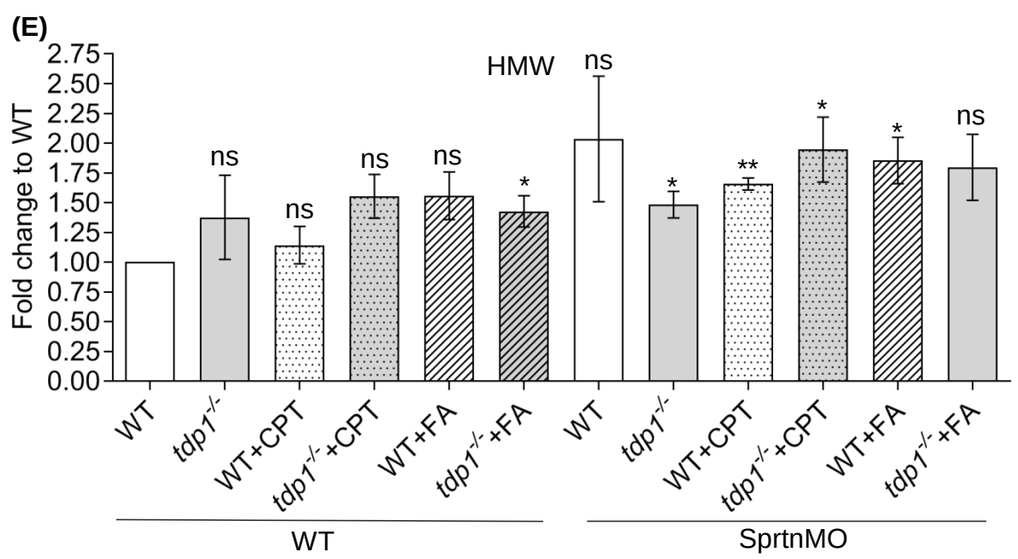
(E)
HMW
Fold change to WT
WT
SprtnMO

Figure 5

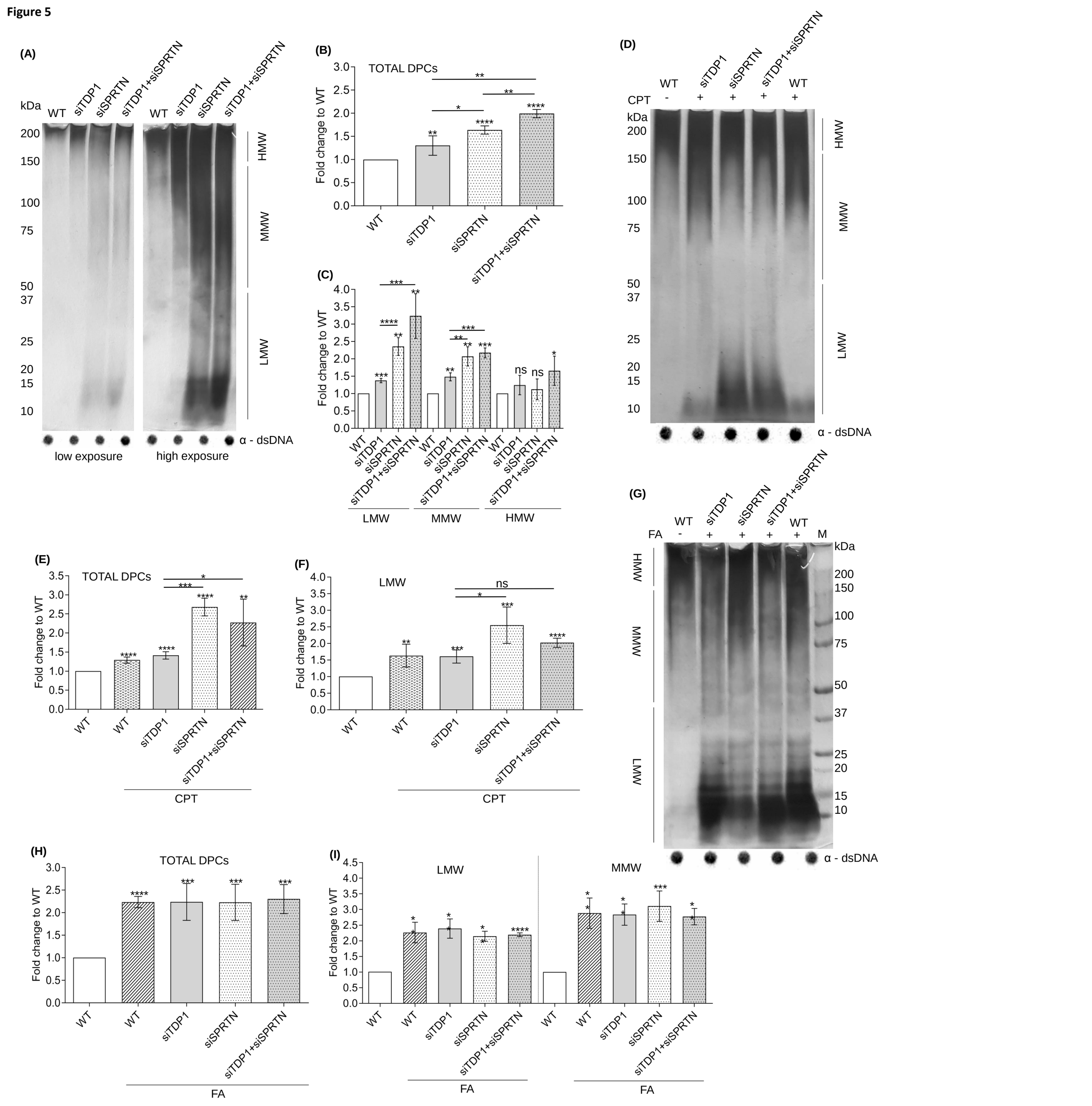
(A)
kDa
WT
siTDP1
siSPRTN
siTDP1+siSPRTN
200
150
100
75
50
37
25
20
15
10
HMW
MMW
LMW
α - dsDNA
low exposure
high exposure
(B)
TOTAL DPCs
Fold change to WT
(C)
Fold change to WT
LMW
MMW
HMW
(D)
CPT
kDa
HMW
MMW
LMW
α - dsDNA
(E)
TOTAL DPCs
Fold change to WT
CPT
(F)
LMW
Fold change to WT
CPT
(G)
FA
M
kDa
HMW
MMW
LMW
α - dsDNA
(H)
TOTAL DPCs
Fold change to WT
FA
(I)
LMW
MMW
Fold change to WT
FA
FA

Figure 6

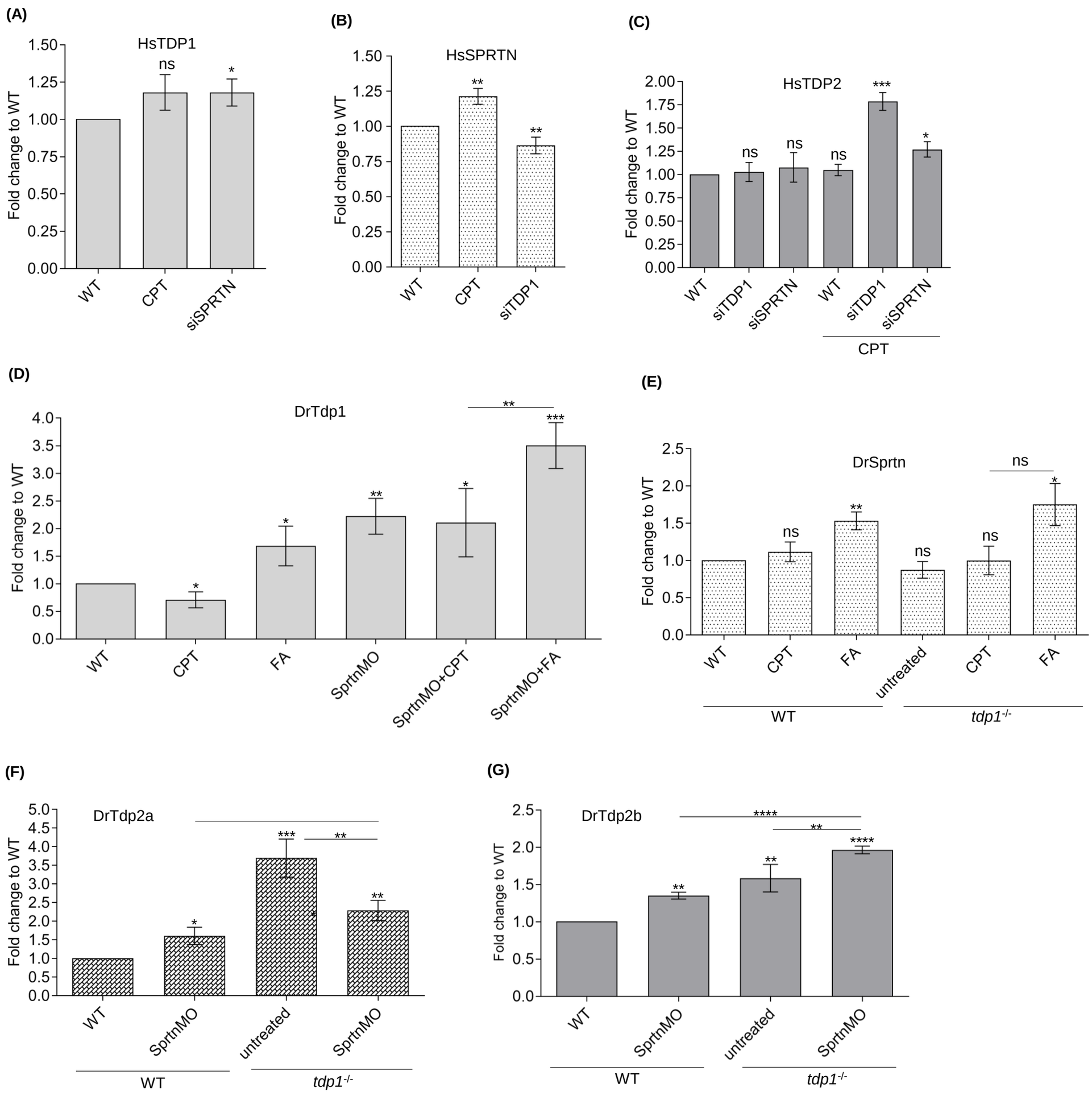
(A)
HsTDP1
Fold change to WT
1.50
1.25
1.00
0.75
0.50
0.25
0.00
ns
*
WT
CPT
siSPRTN
(B)
HsSPRTN
Fold change to WT
**
**
WT
CPT
siTDP1
(C)
HsTDP2
Fold change to WT
2.00
1.75
1.50
1.25
1.00
0.75
0.50
0.25
0.00
ns
ns
ns
***
*
WT
siTDP1
siSPRTN
WT
siTDP1
siSPRTN
CPT
(D)
DrTdp1
Fold change to WT
4.0
3.5
3.0
2.5
2.0
1.5
1.0
0.5
0.0
**
***
*
*
**
*
WT
CPT
FA
SprtnMO
SprtnMO+CPT
SprtnMO+FA
(E)
DrSprtn
Fold change to WT
2.5
2.0
1.5
1.0
0.5
0.0
ns
ns
**
ns
ns
*
WT
CPT
FA
untreated
CPT
FA
WT
tdp1-/-
(F)
DrTdp2a
Fold change to WT
5.0
4.5
4.0
3.5
3.0
2.5
2.0
1.5
1.0
0.5
0.0
***
**
*
**
WT
SprtnMO
untreated
SprtnMO
WT
tdp1-/-
(G)
DrTdp2b
Fold change to WT
2.5
2.0
1.5
1.0
0.5
0.0
****
**
**
**
****
WT
SprtnMO
untreated
SprtnMO
WT
tdp1-/-

Figure 7

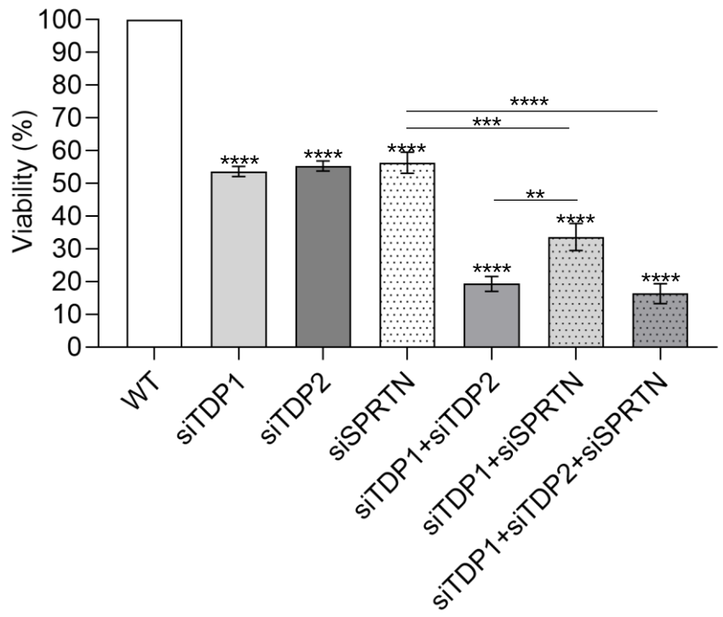
Viability (%)
100
90
80
70
60
50
40
30
20
10
0
****
***
**
WT
siTDP1
siTDP2
siSPRTN
siTDP1+siTDP2
siTDP1+siSPRTN
siTDP1+siTDP2+siSPRTN

Figure 8

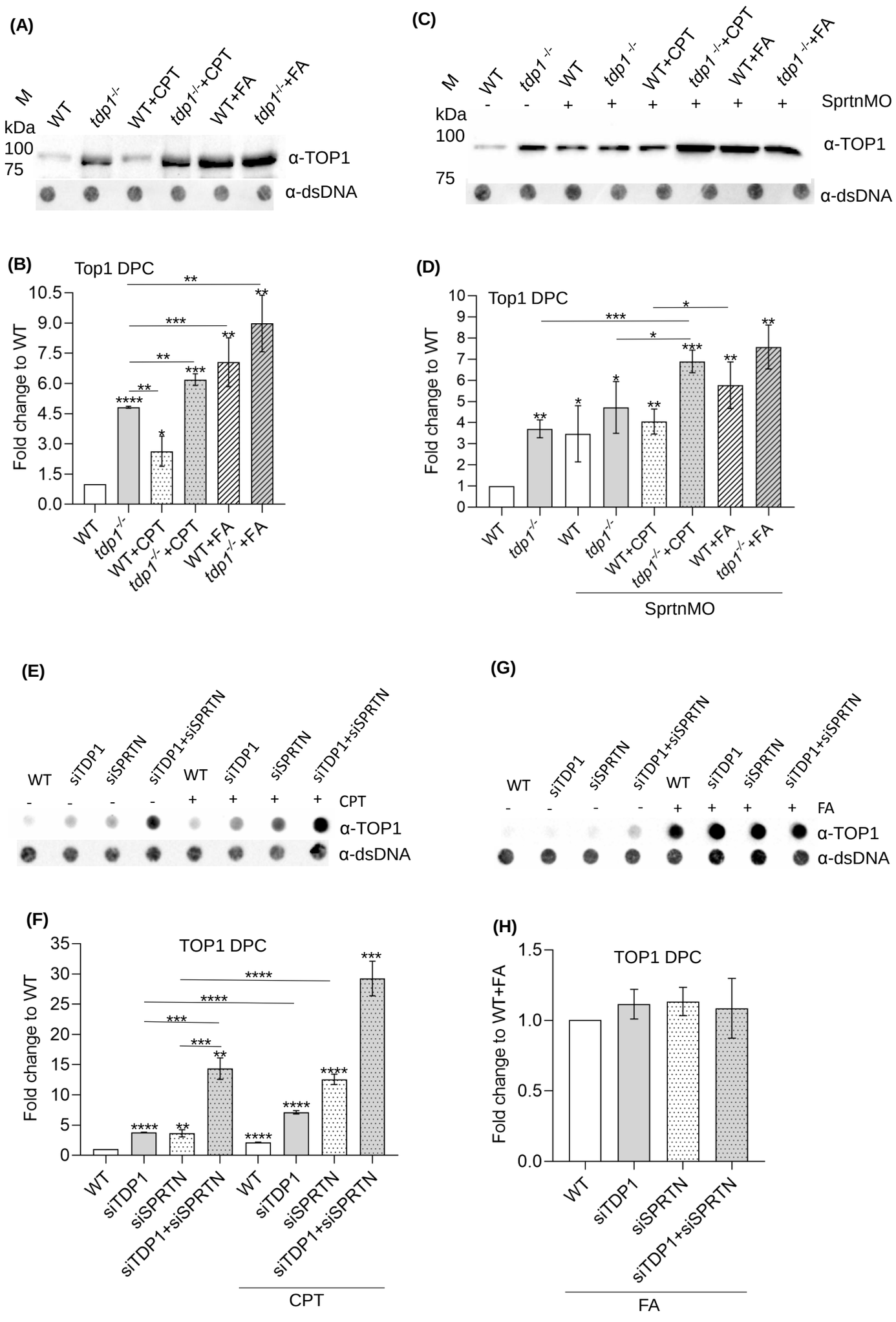
(A)
M
WT
tdp1-/-
WT+CPT
tdp1-/-+CPT
WT+FA
tdp1-/-+FA
kDa
100
75
α-TOP1
α-dsDNA
(C)
SprtnMO
(B)
Top1 DPC
Fold change to WT
(D)
(E)
siTDP1
siSPRTN
siTDP1+siSPRTN
CPT
(G)
FA
(F)
TOP1 DPC
(H)
Fold change to WT+FA

Figure 9

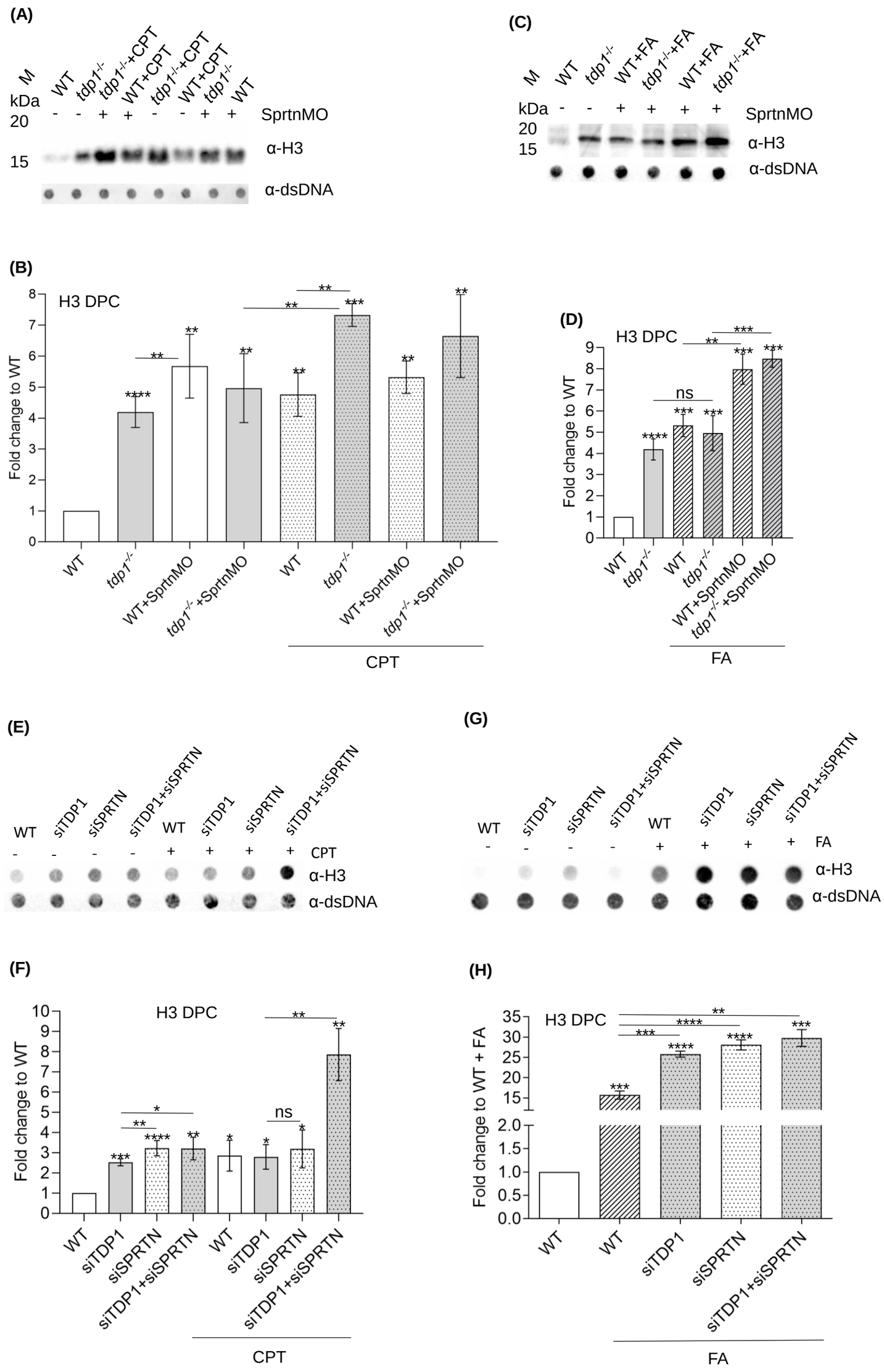
(A)
M
kDa
20
15
WT
tdp1-/-
tdp1-/-+CPT
WT+CPT
tdp1-/-+CPT
WT+CPT
tdp1-/-
WT
SprtnMO
α-H3
α-dsDNA
(C)
WT+FA
tdp1-/-+FA
(B)
H3 DPC
Fold change to WT
WT+SprtnMO
tdp1-/- +SprtnMO
CPT
(D)
ns
FA
(E)
siTDP1
siSPRTN
siTDP1+siSPRTN
CPT
(G)
FA
(F)
(H)
Fold change to WT + FA

Figure S1.

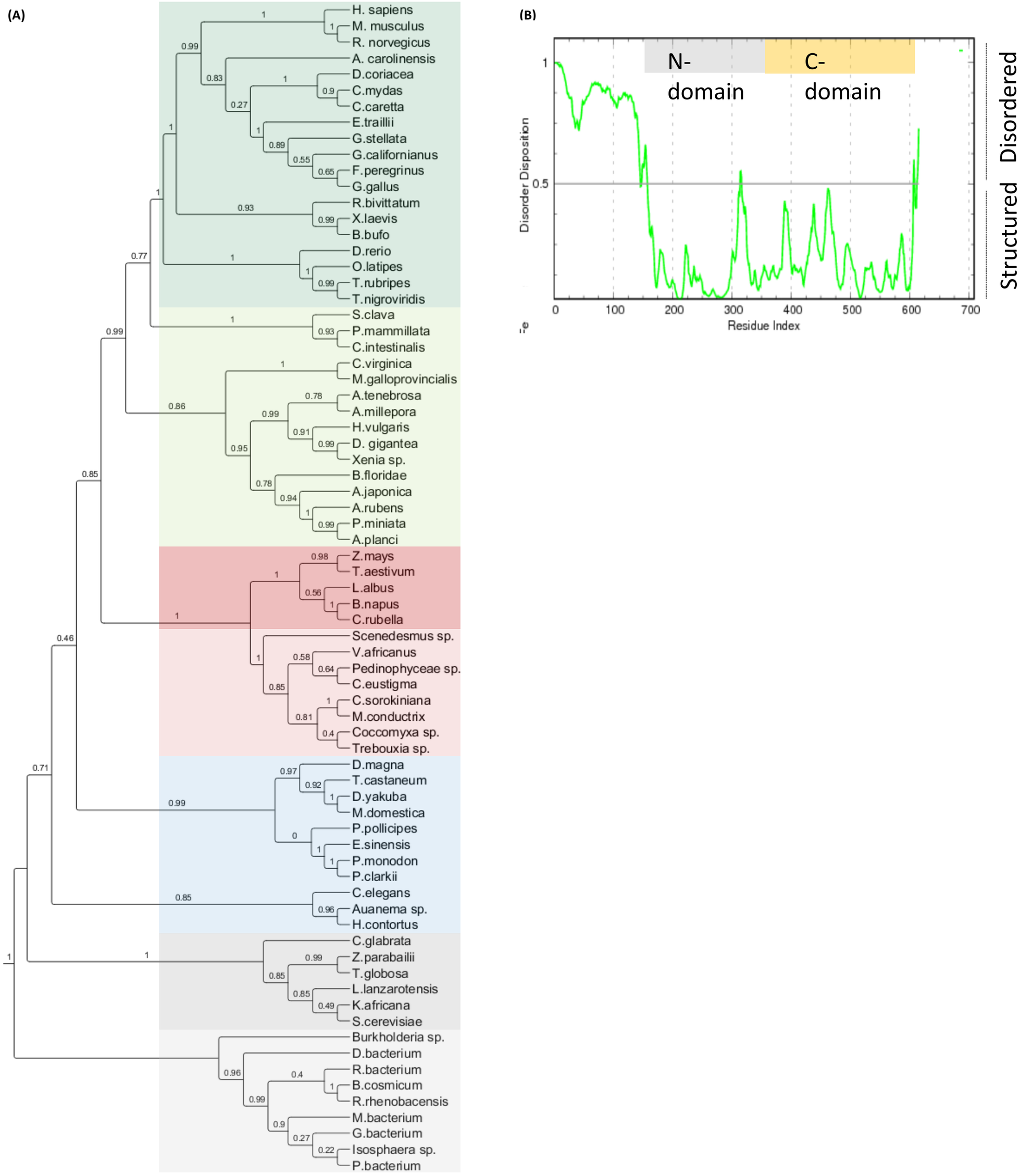
(A)
H. sapiens
M. musculus
R. norvegicus
A. carolinensis
D.coriacea
C.mydas
C.caretta
E.traillii
G.stellata
G.californianus
F.peregrinus
G.gallus
R.bivittatum
X.laevis
B.bufo
D.rerio
O.latipes
T.rubripes
T.nigroviridis
S.clava
P.mammillata
C.intestinalis
C.virginica
M.galloprovincialis
A.tenebrosa
A.millepora
H.vulgaris
D. gigantea
Xenia sp.
B.floridae
A.japonica
A.rubens
P.miniata
A.planci
Z.mays
T.aestivum
L.albus
B.napus
C.rubella
Scenedesmus sp.
V.africanus
Pedinophyceae sp.
C.eustigma
C.sorokiniana
M.conductrix
Coccomyxa sp.
Trebouxia sp.
D.magna
T.castaneum
D.yakuba
M.domestica
P.pollicipes
E.sinensis
P.monodon
P.clarkii
C.elegans
Auanema sp.
H.contortus
C.glabrata
Z.parabailii
T.globosa
L.lanzarotensis
K.africana
S.cerevisiae
Burkholderia sp.
D.bacterium
R.bacterium
B.cosmicum
R.rhenobacensis
M.bacterium
G.bacterium
Isosphaera sp.
P.bacterium
(B)
N-domain
C-domain
Disorder Disposition
Residue Index
Disordered
Structured

Figure S2.

(A)

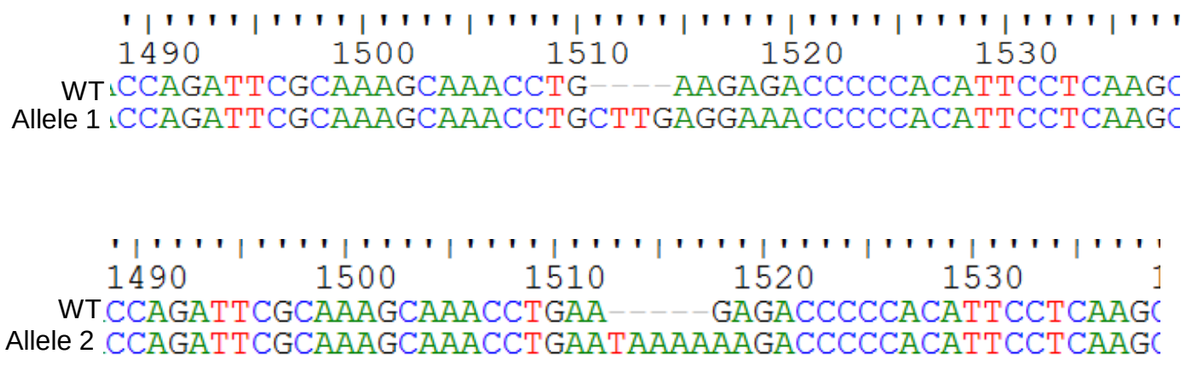
1490 1500 1510 1520 1530
WT CCAGATTCGCAAAGCAAACCTG----AAGAGACCCCCACATTCCTCAAGC
Allele 1 CCAGATTCGCAAAGCAAACCTGCTTGAGGAAACCCCCACATTCCTCAAGC
1490 1500 1510 1520 1530
WT CCAGATTCGCAAAGCAAACCTGAA-----GAGACCCCCACATTCCTCAAGC
Allele 2 CCAGATTCGCAAAGCAAACCTGAATAAAAAAGACCCCCACATTCCTCAAGC

(B)

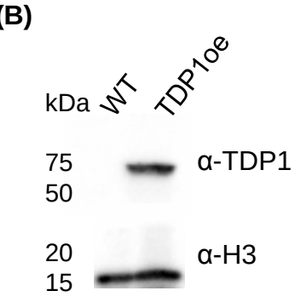
kDa
WT
TDP1oe
75
50
α-TDP1
20
15
α-H3

Figure S3.

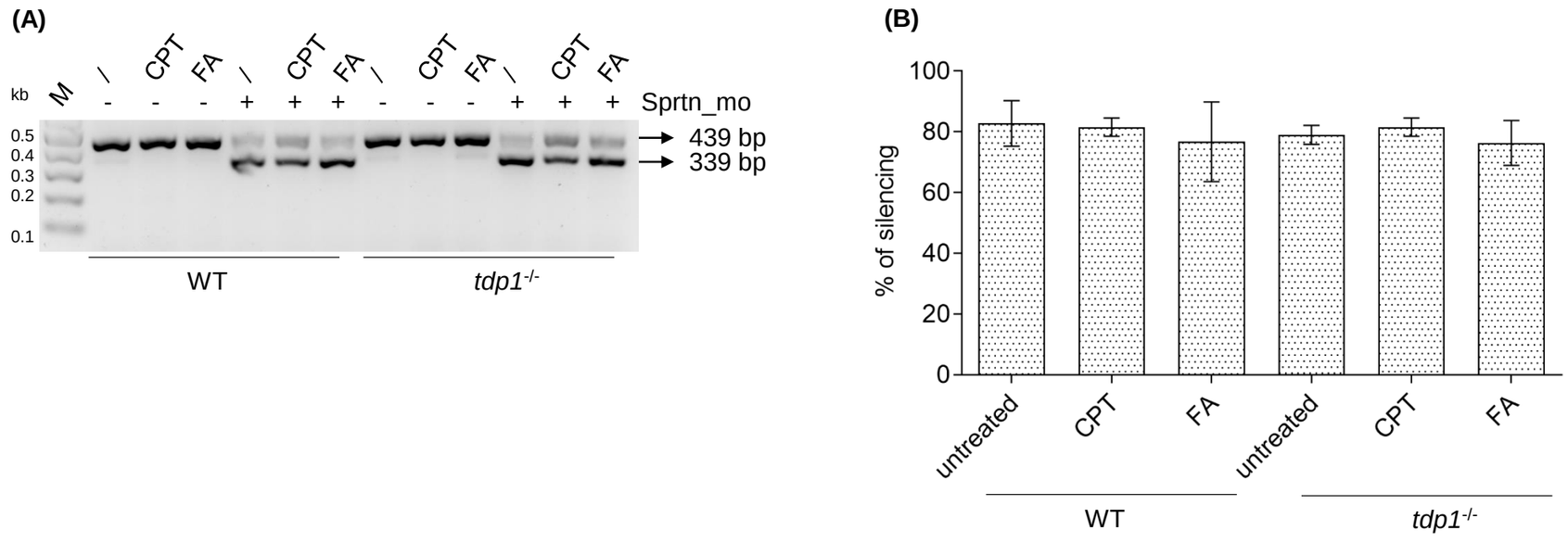
(A)
kb
M
\
CPT
FA
Sprtn_mo
0.5
0.4
0.3
0.2
0.1
439 bp
339 bp
WT
tdp1-/-
(B)
% of silencing
100
80
60
40
20
0
untreated
CPT
FA
WT
tdp1-/-

Figure S4.

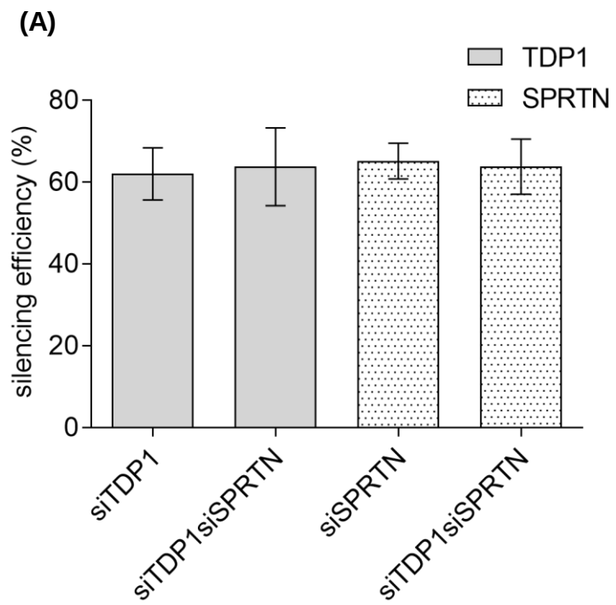
(A)
TDP1
SPRTN
silencing efficiency (%)
80
60
40
20
0
siTDP1
siTDP1siSPRTN
siSPRTN
siTDP1siSPRTN

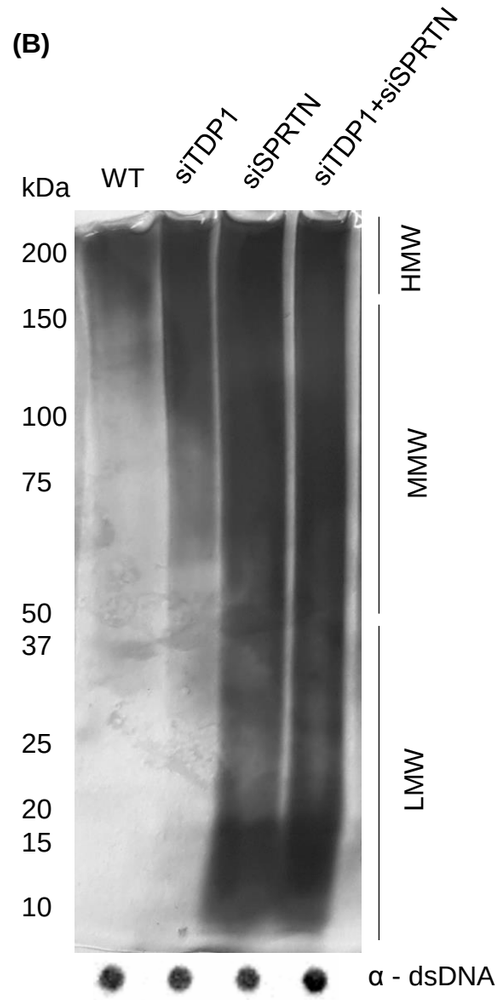
(B)
kDa
WT
siTDP1
siSPRTN
siTDP1+siSPRTN
200
150
100
75
50
37
25
20
15
10
HMW
MMW
LMW
α - dsDNA

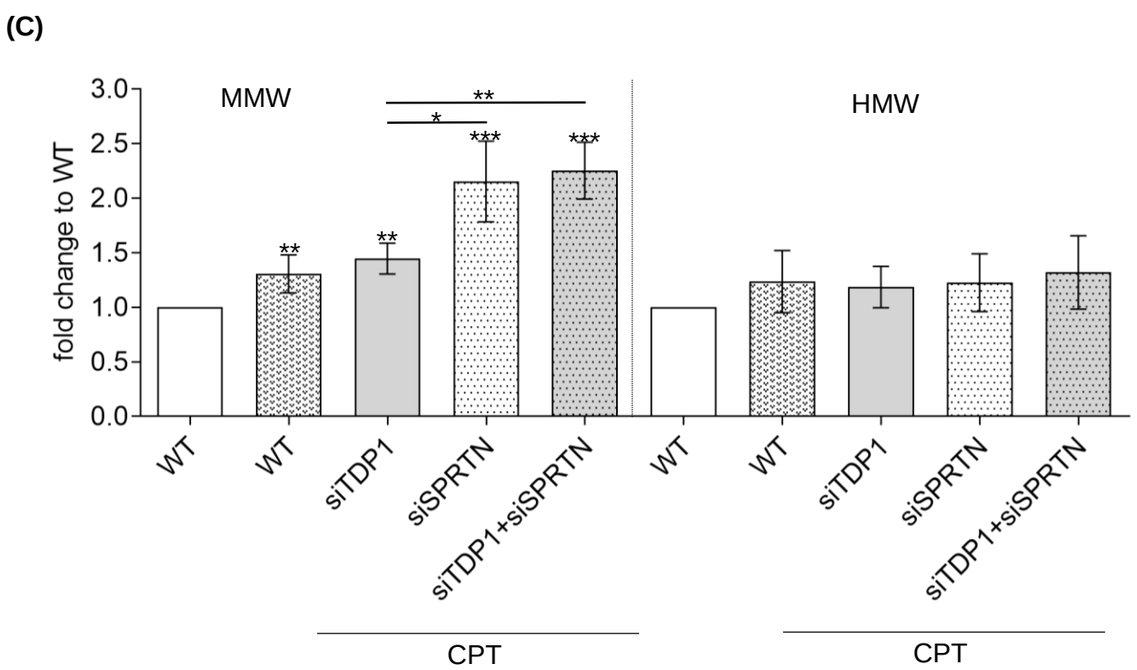
(C)
MMW
HMW
fold change to WT
3.0
2.5
2.0
1.5
1.0
0.5
0.0
**
*
***
***
**
**
WT
WT
siTDP1
siSPRTN
siTDP1+siSPRTN
WT
WT
siTDP1
siSPRTN
siTDP1+siSPRTN
CPT
CPT

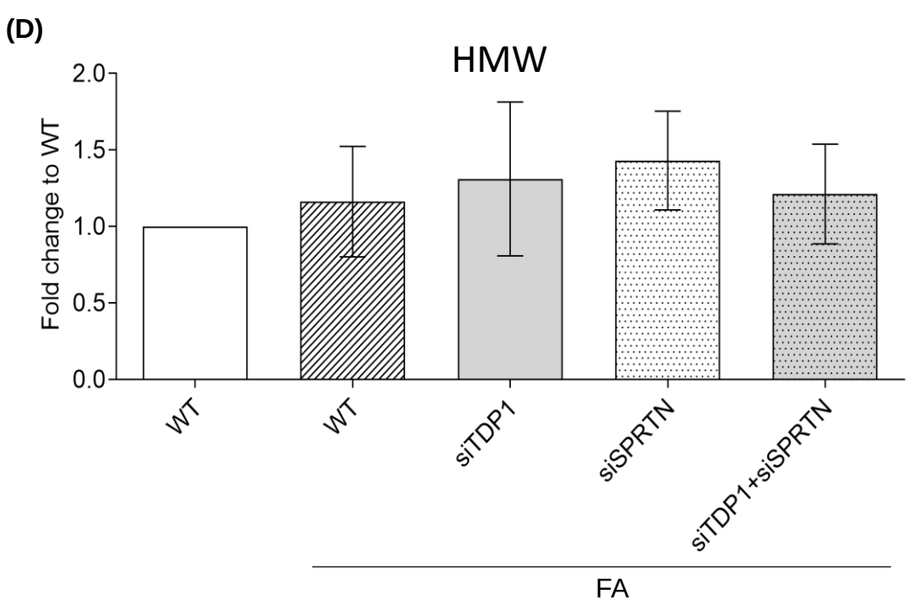
(D)
HMW
Fold change to WT
2.0
1.5
1.0
0.5
0.0
WT
WT
siTDP1
siSPRTN
siTDP1+siSPRTN
FA

Figure S5.

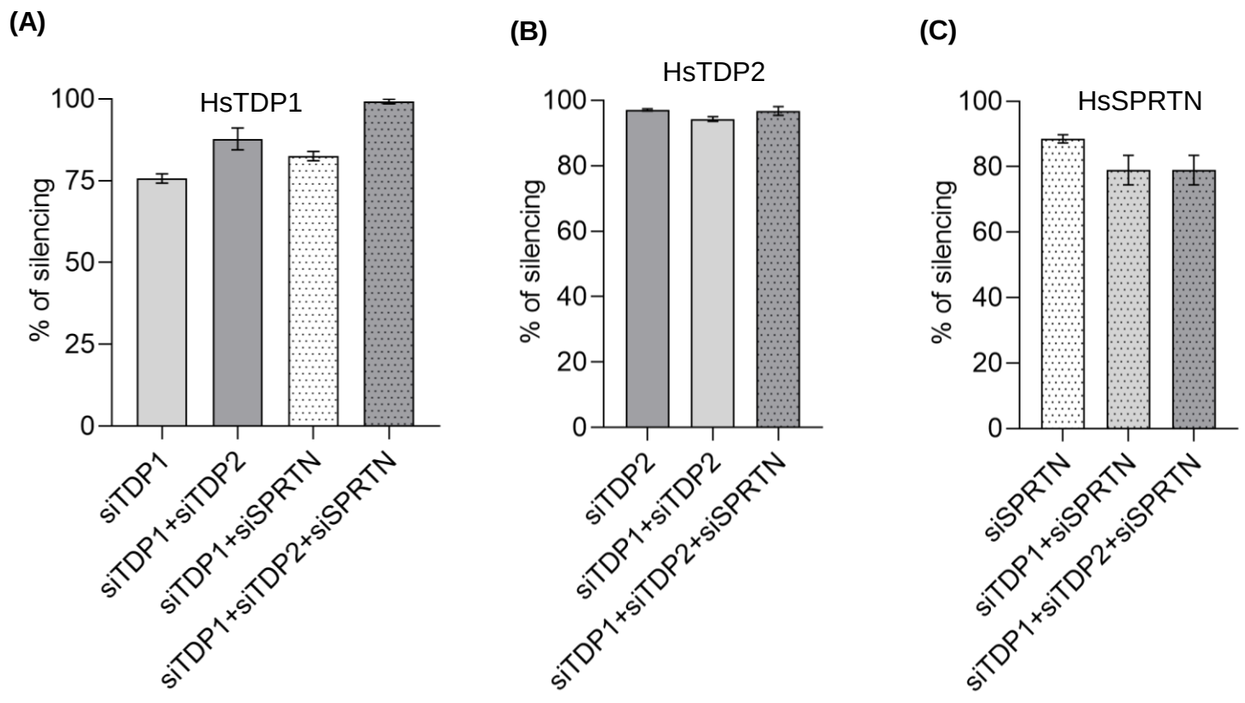
(A)
HsTDP1
% of silencing
100
75
50
25
0
siTDP1
siTDP1+siTDP2
siTDP1+siSPRTN
siTDP1+siTDP2+siSPRTN
(B)
HsTDP2
% of silencing
100
80
60
40
20
0
siTDP2
siTDP1+siTDP2
siTDP1+siTDP2+siSPRTN
(C)
HsSPRTN
% of silencing
100
80
60
40
20
0
siSPRTN
siTDP1+siSPRTN
siTDP1+siTDP2+siSPRTN

Figure S6.

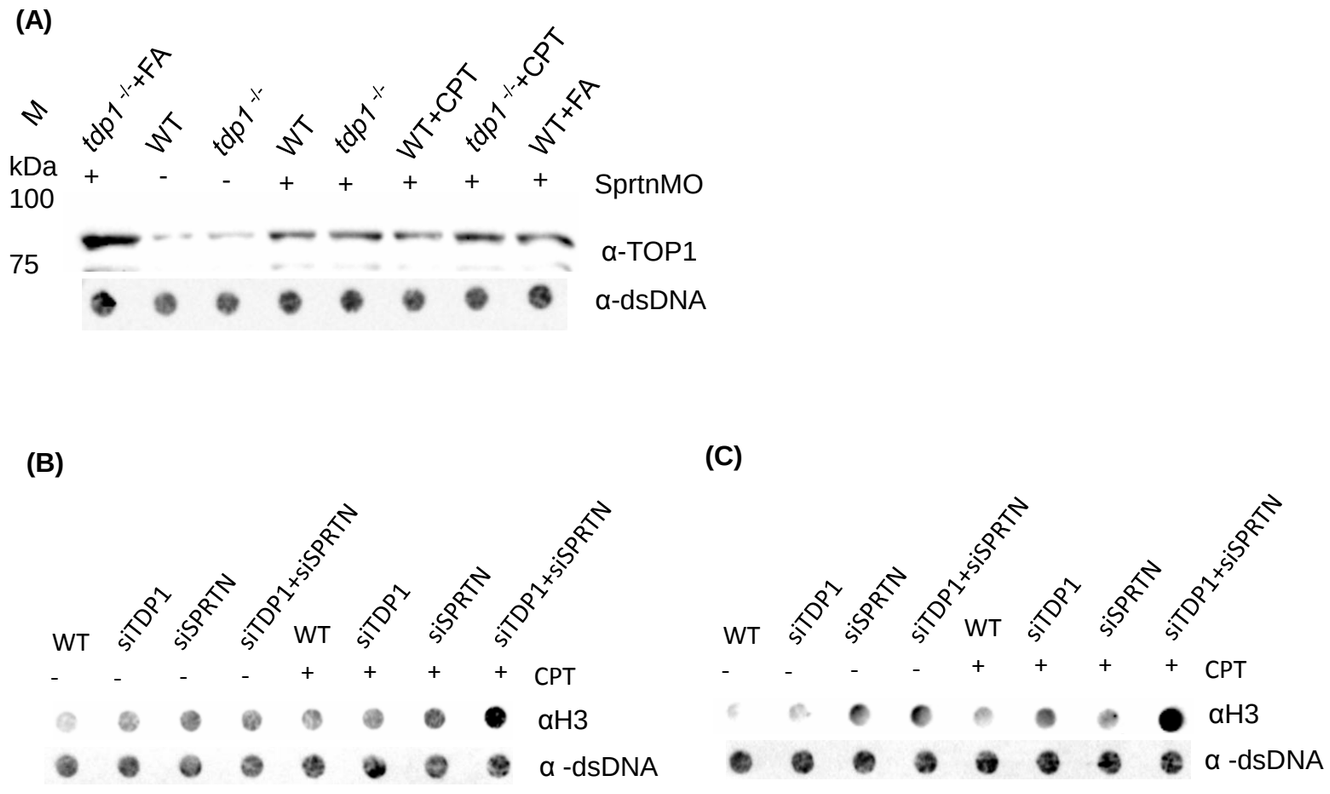
(A)
M
tdp1 -/-+FA
WT
tdp1 -/-
WT
tdp1 -/-
WT+CPT
tdp1 -/-+CPT
WT+FA
kDa
100
+ - - + + + + +
SprtnMO
75
α-TOP1
α-dsDNA
(B)
WT
siTDP1
siSPRTN
siTDP1+siSPRTN
WT
siTDP1
siSPRTN
siTDP1+siSPRTN
- - - - + + + +
CPT
αH3
α -dsDNA
(C)
WT
siTDP1
siSPRTN
siTDP1+siSPRTN
WT
siTDP1
siSPRTN
siTDP1+siSPRTN
- - - - + + + +
CPT
αH3
α -dsDNA

Table S1.

Abbreviation	Accession no.	Species	Group
H.sapiens	NP_060789.2	Homo sapiens	mammals
M.musculus	XP_030102367.1	Mus musculus	mammals
R.norvegicus	XP_006240494.1	Rattus norvegicus	mammals
G.gallus	XP_040528900.1	Gallus gallus	birds
F.peregrinus	XP_005241969.1	Falco peregrinus	birds
G.stellata	XP_009818907.1	Gavia stellata	birds
G.californianus	XP_050754186.1	Gymnogyps californianus	birds
E.traillii	XP_027758233.1	Empidonax traillii	birds
A.carolinensis	XP_003214461.1	Anolis carolinensis	reptiles
C.mydas	XP_037756745.1	Chelonia mydas	reptiles
D.coriacea	XP_038262859.1	Dermochelys coriacea	reptiles
C.caretta	XP_048709928.1	Caretta caretta	reptiles
X.laevis	NP_001087094.1	Xaneopus laevis	amphibians
R.bivittatum	XP_029453633.1	Rhinatrema bivittatum	amphibians
B.bufo	XP_040268057.1	Bufo bufo	amphibians
D.rerio	XP_700174.2	Danio rerio	fish
O.latipes	XP_023809425.1	Oryzias latipes	fish
T.rubripes	XP_003969465.3	Takifugu rubripes	fish
T.nigroviridis	CAG03090.1	Tetraodon nigroviridis	fish
B.floridae	XP_035693489.1	Branchiostoma floridae	chordata
P.mammillata	CAB3266878.1	Phallusia mammillata	tunicata
S.clava	XP_039264827.1	Styela clava	tunicata
C.intestinalis	XP_002123899.2	Ciona intestinalis	tunicata
P.miniata	XP_038045909.1	Patiria miniata	echinodermata
A.japonica	XP_033125892.1	Anneissia japonica	echinodermata
A.planci	XP_022107496.1	Acanthaster planci	echinodermata
A.rubens	XP_033639145.1	Asterias rubens	echinodermata
D.yakuba	XP_039227154.1	Drosophila yakuba	insecta
M.domestica	XP_005187304.1	Musa domestica	insecta
T.castaneum	XP_008191977.1	Triboleum castaneum	insecta
D.magna	KZS04356.1	Daphnia magna	crustacea
P.monodon	XP_037795115.1	Penaeus monodon	crustacea
P.clarkii	XP_045608059.1	Procambarus clarkii	crustacea
E.sinensis	XP_050707432.1	Eriocheir sinensis	crustacea
P.pollicipes	XP_037088035.1	Pollicipes pollicipes	crustacea
C.virginica	XP_022329852.1	Crassostrea virginica	mollusca
M.galloprovincialis	VDI74315.1	Mytilus galloprovincialis	mollusca
C.elegans	NP_500149.1	Caenorhabditis elegans	nematoda
Auanema sp.	CAH6628979.1	Auanema sp. JU1783	nematoda
H.contortus	CDJ85118.1	Haemonchus contortus	nematoda
A.tenebrosa	XP_031555938.1	Actinia tenebrosa	cnidaria
A.millepora	XP_029211704.2	Acropora millepora	cnidaria
D. gigantea	XP_028398530.1	Dendronephthya gigantea	cnidaria
Xenia sp.	XP_046847875.1	Xenia sp. Carnegie-2017	cnidaria
H.vulgaris	XP_047136116.1	Hydra vulgaris	cnidaria
Z.mays	NP_001169273.1	Zea mays	plant
T.aestivum	XP_044456423.1	Triticum aestivum	plant
B.napus	XP_013728150.2	Brassica napus	plant
L.albus	KAE9606436.1	Lupinus albus	plant
C.rubella	XP_006290125.2	Capsella rubella	plant
L.lanzarotensis	XP_022629229.1	Lachancea lanzarotensis	fungi
Z.parabailii	AQZ17865.1	Zygosaccharomyces parabailii	fungi
T.globosa	XP_037141659.1	Torulaspora globosa	fungi
K.africana	XP_003958391.1	Kazachstania africana	fungi
C.glabrata	KAH7582295.1	Candida glabrata	fungi
S.cerevisiae	AJQ13221.1	Saccharomyces cerevisiae	yeast
D.bacterium	MBI1948579.1	Deltaproteobacteria bacterium	bacteria
Burkholderia sp.	WP_226115822.1	Burkholderia sp. AU33545	bacteria
B.cosmicum	WP_143845348.1	Bradyrhizobium cosmicum	bacteria
R.rhenobacensis	WP_184254289.1	Rhodopseudomonas rhenobacensis	bacteria
Isosphaera sp.	MBA4064840.1	Isosphaera sp.	bacteria
P.bacterium	MBA4190599.1	Planctomycetaceae bacterium	bacteria
M.bacterium	MBK7077015.1	Myxococcales bacterium	bacteria
G.bacterium	OGS99019.1	Gallionellales bacterium	bacteria
R.bacterium	SEP49348.1	Rhodospirillales bacterium	bacteria
C.eustigma	GAX84131.1	Chlamydomonas eustigma	algae
C.sorokiniana	PRW59620.1	Chlorella sorokiniana	algae
Pedinophyceae sp.	CAG9462817.1	Pedinophyceae sp. YPF-701	algae
Scenedesmus sp.	KAF8054979.1	Scenedesmus sp. PABB004	algae
Trebouxia sp.	KAA6424393.1	Trebouxia sp. A1-2	algae
M.conductrix	PSC74986.1	Micractinium conductrix	algae
V.africanus	GIL60588.1	Volvox africanus	algae
Coccomyxa sp.	BDA43991.1	Coccomyxa sp. Obi	algae